Miner Deposita (2017) 52:845–862
DOI 10.1007/s00126-016-0703-7

ARTICLE

Lithological and geochemical constraints on the magma conduit systems of the Huangshan Ni-Cu sulfide deposit, NW China

Yu-Feng Deng[1,2] · Xie-Yan Song[3] · Pete Hollings[1,4] · Lie-Meng Chen[3] · Taofa Zhou[1,2] · Feng Yuan[1,2,5] · Wei Xie[6] · Dayu Zhang[1,2] · Bingbing Zhao[1]

Received: 8 January 2016 / Accepted: 28 November 2016 / Published online: 23 December 2016

Abstract Magmatic Ni-Cu sulfide deposits in northern Xinjiang, China, are associated with small mafic-ultramafic complexes, with the sulfide ores generally occurring in ultramafic rocks. The Huangshan deposit (up to 65 Mt of ore at 0.49% Ni and 0.31% Cu), one of the largest magmatic Ni-Cu deposits in northern Xinjiang, is composed of a layered sequence of lower websterite, lower lherzolite, websterite, norite-gabbro, gabbro, diorite, and gabbronorite, with sulfide mineralization mainly found in the lower lherzolite, lower websterite, and websterite. Systematic variations of the major oxides and trace elements suggest that the rocks of the Huangshan deposit are fractionated from the same parental magma, with the sharp contact and discontinuous trends of major oxide contents between different lithologies implying intrusion of four distinct stages of magma from a single deep-seated staging chamber. The reversals in olivine Fo contents and major oxides in the lower lherzolite were the result of inhomogeneity in olivine within the lower chamber. The Se/S ratios (63.1~150 × 10^{-6}) and the negative correlation between Se/S and $\delta^{34}S$ (0.63~2.42‰) of the sulfide ores suggest that a large contribution of crustal S caused the sulfide segregation. The sulfides in the lower lherzolite have lower Cu contents (1386–2200 ppm) and Cu/Pd ratios (2.31 × 10^5–1.36 × 10^6) relative to those in the mineralized lower websterite (Cu = 2300 to 18,700 ppm, and Cu/Pd = 6.65 × 10^5 to 2.73 × 10^6). A positive correlation between Pd/Ir and Ni/Ir for the vein-textured sulfides in the lower websterite likely reflects fractionated sulfides picked up by a new pulse of magma. In contrast, the restricted range of Pd/Ir ratios indicates that the PGE contents of the disseminated sulfides in the lower lherzolite resulted from reaction between the sulfides and new pulses of S-undersaturated magma.

Keywords Magmatic Ni-Cu sulfide deposit · Central Asian Orogenic Belt · Huangshan mafic-ultramafic intrusion · Magma conduit system · Sulfide saturation

Editorial handling: M. Fiorentini

Electronic supplementary material The online version of this article (doi:10.1007/s00126-016-0703-7) contains supplementary material, which is available to authorized users.

✉ Xie-Yan Song
songxieyan@vip.gyig.ac.cn

[1] School of Resources and Environmental Engineering, Hefei University of Technology, Hefei 230009, China

[2] Ore Deposit and Exploration Centre, Hefei University of Technology, Hefei 230009, China

[3] State Key Laboratory of Ore Deposit Geochemistry, Institute of Geochemistry, Chinese Academy of Sciences, 46th Guanshui Road, Guiyang 550002, People's Republic of China

[4] Department of Geology, Lakehead University, 955 Oliver Road, Thunder Bay, ON P7B 5E1, Canada

[5] Xinjiang Research Centre for Mineral Resources, Xinjiang Institute of Ecology and Geography, Chinese Academy of Sciences, Urumqi, Xinjiang 830011, China

[6] State Key Laboratory of Isotope Geochemistry, Guangzhou Institute of Geochemistry, Chinese Academy of Sciences, Guangzhou 510640, China

Introduction

Several magmatic Ni-Cu deposits are hosted in Permian mafic-ultramafic intrusions in northern Xinjiang, NW China, within the Phanerozoic Central Asian Orogenic Belt (CAOB; Fig. 1). The main deposits include Kalatongke, Huangshandong, Huangshan, Tulaergen, and Poyi with a total Ni metal reserve of approximately two million tons, making

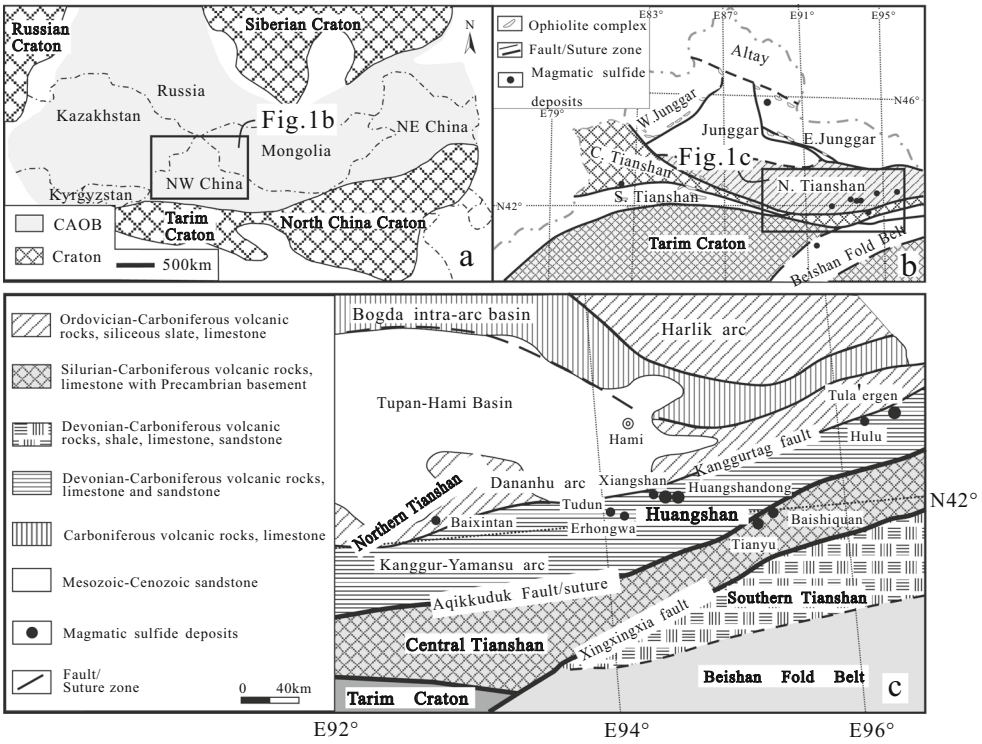

Fig. 1 **a** Schematic geological map of the Central Asian Orogenic Belt (after Jahn et al. 2000 and Xiao et al. 2009); **b** tectonic units of northern Xinjiang (after BGMX 1993); **c** simplified geological map of Northern Tianshan (after BGMX 1993; Xiao et al. 2004; Song et al. 2011, 2013)

northern Xinjiang the second largest Ni resource in China after Jinchuan (Qin et al. 2003; Liu et al. 2005; Xia et al. 2013). The intrusions hosting the deposits typically have a surface area of less than 10 km^2 and mainly consist of dunite, lherzolite, harzburgite, websterite, and gabbro with rare norite found at the margins and bases. The Ni-Cu sulfides are dominantly hosted in ultramafic rocks, as in the Huangshan, Huangshandong, Tuerlagen, and Poyi deposits (Qin et al. 2003; Liu et al. 2005). The mantle source and tectonic setting of these intrusive rocks have been extensively studied (Gu et al. 2006; Mao et al. 2008; Pirajno et al. 2008; Qin et al. 2011; Su et al. 2011, 2012; Sun et al. 2013; Tang et al. 2013; Song et al. 2013; Gao et al. 2013; Deng et al. 2014, 2015; Mao et al. 2014, 2015) with some studies proposing that the Ni-Cu sulfide deposits formed in magma conduit systems (Su et al. 2013; Gao et al. 2013; Mao et al. 2014, 2015).

The Huangshan intrusion (also referred to as Huangshanxi in the literature) is a small mafic-ultramafic intrusion that hosts the second largest Ni-Cu sulfide deposit in northern Xinjiang. Gabbros from the intrusion have yielded crystallization ages of 284.5 ± 2.5 and 283.8 ± 3.4 Ma by zircon U-Pb LA-ICP-MS and TIMS (Gu et al. 2006; Qin et al. 2011). The intrusion is believed to have formed either from plume-related magmatism or interaction between metasomatized lithospheric mantle and ascending asthenospheric mantle as a result of slab break-off (Zhou et al. 2004; Su et al. 2011; Song et al. 2013; Deng et al. 2015). Mass balance calculations for incompatible trace elements and sulfide abundances suggest that the Huangshan intrusion represents a dynamic magma conduit (Zhang et al. 2011). Assimilation of S-bearing crust and fractional crystallization likely played an important role in sulfide saturation (Zhou et al. 2004; Zhang et al. 2011; Tang et al. 2012; Mao et al. 2014). However, some important issues are not fully understood, including (1) the mechanism of reversals of olivine and whole-rock composition in the lower lherzolite and lower websterite, (2) the causes of sulfide saturation, and (3) origin of sulfide mineralization in the lower lherzolite and lower websterite. In this study, we investigate the role of magma conduit systems in the formation of the different lithofacies and sulfide ores in the Huangshan intrusion using lithology, mineral, and whole-rock geochemistry.

Geological background

The CAOB formed by amalgamation of microcontinents and arc accretion prior to the Early Permian or Early Triassic (Windley et al. 2007; Xiao et al. 2008, 2009). It extends from Kazakhstan in the west to eastern Siberia in the east and separates the Siberian Craton in the north from the Tarim-North China Craton in the south (Fig. 1a; Sengör et al. 1993; Jahn et al. 2000, Jahn 2004; Windley et al. 2007; Xiao et al. 2004, 2008). The southern CAOB in northwest China is composed of, from north to the south, the Chinese Altai, Junggar, and Tianshan terranes as well as the Beishan Fold Belt (Fig. 1b). The Tianshan terrane can be further divided into three tectonic units: the Northern, Central, and Southern Tianshan (Fig. 1c; BGMX 1993; Xiao et al. 2004, 2008; Zhou et al. 2010; Zhang et al. 2013, 2014).

A number of magmatic Ni-Cu sulfide deposits have been discovered on the northern margin of the Junggar terrane, in the Central Tianshan terrane, the Beishan fold belt, and the Northern Tianshan terrane (Fig. 1; Mao et al. 2008; Qin et al. 2011; Song et al. 2011, 2013; Gao and Zhou 2012, Gao et al. 2013; Sun et al. 2013; Xia et al. 2013; Deng et al. 2014). Recent discoveries include a Ni-Cu sulfide deposit hosted in the Permian Poyi ultramafic intrusion in the Beishan fold belt that has been estimated to contain 1.3 million metric tons of Ni and 220,000 t of Cu (Xia et al. 2013), and Ni-Cu mineralization in the Permian Baixintan mafic-ultramafic intrusion (Fig. 1c; Wang et al. 2015). Though most of these deposits formed in the Early Permian in Northern Xinjiang, a few Ni-Cu sulfide mineralized intrusions, such as the Carboniferous Tulargen intrusion (San et al. 2010; Jiao et al. 2012) and the Silurian Jingbulake intrusion (Yang and Zhou 2009) are also located in the Northern and Central Tianshan terranes. More than 30 Early Permian mafic-ultramafic intrusions have been identified along the east-trending Kanggurtag fault in the Northern Tianshan, eight of which host magmatic Ni-Cu sulfide deposits (Fig. 1c; Mao et al. 2008; San et al. 2010; Qin et al. 2011; Song et al. 2013; Su et al. 2013; Sun et al. 2013; Wang et al. 2015). The Huangshan and Huangshandong Ni-Cu sulfide deposits are located in the eastern part of the Northern Tianshan and are associated with kilometer-scale tension gashes generated by Permian dextral shearing (Branquet et al. 2012).

Petrography of the Huangshan intrusion

The Huangshan intrusion is ~2.5 km long and ~50–400 m wide and was emplaced into the early Carboniferous siltstone, limestone, and altered basalt of the Gandun Formation (Fig. 2; Li et al. 1989). The limestones have been metamorphosed to garnet-diopside-wollastonite marble close to the intrusion and can be found as xenoliths within it (Wang et al. 1987). The Huangshan intrusion is predominantly composed of a basal gabbronorite (>200 m thick); lower websterite (0–100 m thick); lower lherzolite (100–450 m thick); a middle mafic-ultramafic unit (300–600 m thick) consisting of from bottom to top a websterite, norite-gabbro, gabbro, diorite; and an upper lherzolite (0–50 m thick). The upper lherzolite is crosscut by the norite-gabbro of the middle unit (Li et al. 1989). The contacts between the rocks of the middle unit are generally gradational. The lower websterite has a gradational contact with the lower lherzolite and was previously interpreted to be a part of lower lherzolite occurring at the base of that unit. However, its olivine contents (30–35%) are lower than those of lower lherzolite (50–70%), and consequently, it has been reclassified as the lower websterite (Fig. 3a–d; Mao et al. 2014). The contacts between the websterite of the middle unit and the lower lherzolite are sharp. The basal gabbronorite is observed to crosscut the websterite in the middle unit and the lower lherzolite (Fig. 2).

The upper lherzolite contains 60–80% olivine, 10–15% plagioclase, 10–15% hornblende, 0–2% clinopyroxene, 3–5% orthopyroxene, and 1–2% phlogopite. Olivines are enclosed in orthopyroxene, hornblende, and phlogopite. Hornblende and plagioclase are commonly interstitial to other silicates (Wang et al. 1987; Mao 2014). In the middle unit, websterite is composed of 20–35% olivine, 15–50% orthopyroxene, 10–25% clinopyroxene, 5–15% hornblende, 2–15% sulfide, and 0–3% plagioclase (Fig. 3b, d). Some granular clinopyroxenes and orthopyroxenes have reaction coronae of hornblende (Fig. 3e). The sulfides are commonly interstitial to the silicates, but small rounded sulfide inclusions can also be found in olivine crystals. The diorite contains 5–15% quartz, 40–70% plagioclase, and 5–15% biotite. Some biotites have been altered into chlorite (Li et al. 1989). The lower lherzolite contains 50–70% olivine, 5–25% orthopyroxene, 0–15% clinopyroxene, 5–15% hornblende, 2–25% sulfide, and minor phlogopite (Fig. 3a, c). Olivine crystals are euhedral/subhedral and enclosed in large orthopyroxene, clinopyroxene, plagioclase, and hornblende crystals. Orthopyroxene is intergrown with clinopyroxene or enclosed in clinopyroxene and hornblende. The sulfides are commonly interstitial among the silicates whereas trace Cr-spinel is present as small inclusions in silicate minerals (Fig. 3c). In general, olivine (from 50 to 70%) and orthopyroxene abundances (from 5 to 25%) in the lower lherzolite decrease gradually with depth, whereas clinopyroxene (from 0 to 15%) increases (Fig. 4). The lower websterite is composed of 30–35% olivine, 5–15% orthopyroxene, 15–35% clinopyroxene, 5–15% hornblende, and 2–30% sulfide. Some clinopyroxene and olivine crystals are enclosed in sulfide (Fig. 3e). In the lower lherzolite and lower websterite, some olivines and pyroxenes have been altered into serpentine and talc, and some hornblendes have been altered into chlorites (Fig. 3). The basal gabbronorite consists of 50–55% plagioclase, 15–20% orthopyroxene, 10–15% clinopyroxene, 5–15% hornblende, and 1–3% phlogopite plus minor sulfide (1–3%; Fig. 3f). The minerals in some of the websterites in the middle unit and all of the lower websterite have been deformed (Fig. 3b, d). Some hornblende and phlogopite in the basal gabbronorite have been altered to chlorite. The variation in the mineral content between the lower websterite and the lower lherzolite is relatively gradational, whereas between the websterite, lower lherzolite, and basal gabbronorite, it is sharp (Fig. 4).

Sulfide mineralization in the Huangshan deposit

The Huangshan deposit contains 0.32 Mt Ni and 0.18 Mt Cu with average grades of 0.49 wt% Ni and 0.31 wt% Cu (Qin et al. 2003; Zhang et al. 2011). The Ni-Cu sulfide ore bodies

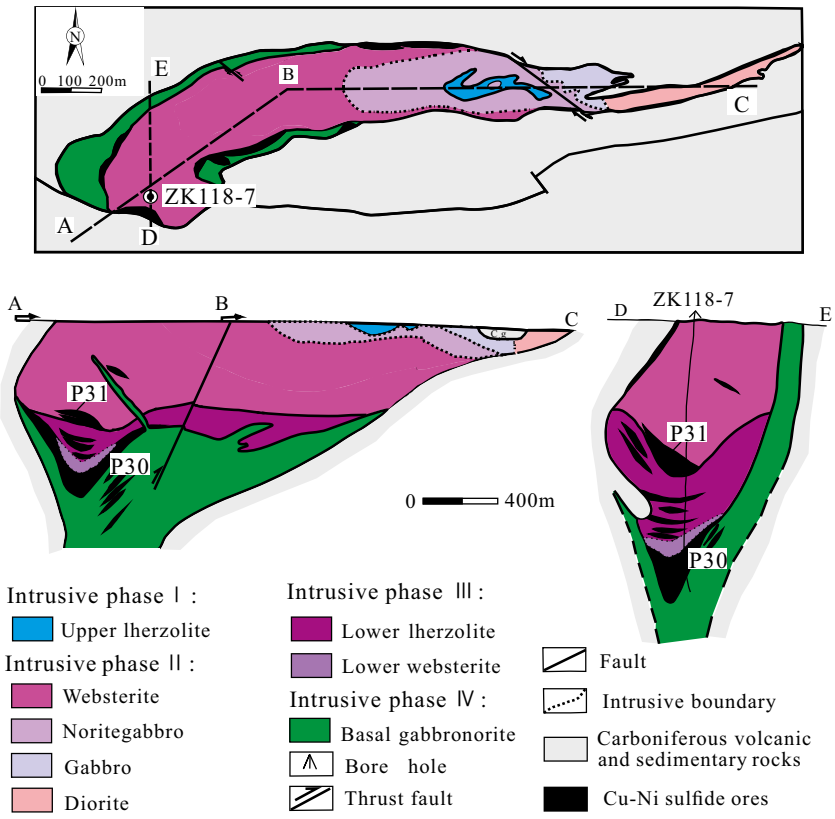

Fig. 2 Simplified geological map and cross sections of the Huangshan intrusion, showing the distribution of lithological units, the P30 and P31 sulfide ore bodies, and the bore hole ZK118-7 (after Li et al. 1989)

are dominantly hosted at the base of lower websterite, lower lherzolite, and websterite. A few small sulfide veins occur in the underlying basal gabbronorite (Fig. 2). The largest ore body (P30) occurs in the lower lherzolite and lower websterite and contains approximately 85% of the total tonnage in the Huangshan deposit, whereas the second largest ore body (P31) is located in the lowermost of the websterite layers and contains about 10% of the total tonnage (Fig. 2; Li et al. 1989). There are also small multilayer ore bodies overlying the P30 ore body (Fig. 2).

The sulfide ores in the lower websterite are mainly net-textured and vein-textured and contain pyrrhotite ± chalcopyrite ± pentlandite (Figs. 3a, b, e and 5a, b). However, in the lower lherzolite and websterite, the sulfides are dominantly disseminated sulfides and comprise pyrrhotite-pentlandite ± chalcopyrite, with less chalcopyrite than in the lower websterite (Fig. 5c, d). Massive sulfide ores are rare and cut across the disseminated sulfide ores in the Huangshan deposit (Mao 2014). Some pentlandites occur as oriented lamellae or along fractures in pyrrhotite grains (Fig. 5d).

Analytical methods

Nineteen samples were collected from the underground mine and drill core (ZK118-7). The units sampled include lower lherzolite, lower websterite, websterite of the middle unit, and basal gabbronorite (Figs. 2 and 4). Sulfide ores from the lower websterite were also sampled.

Olivine was analyzed by wavelength-dispersive X-ray analysis using an EPMA-1600 electron microprobe at the State Key Laboratory of Ore Deposit Geochemistry (SKLODG), the Institute of Geochemistry, Chinese Academy of Sciences. The accelerating voltage was 15 kV, the beam current was 20 nA, and the counting time was set at 10 s. Standard Program International mineral standards (USA) were used for calibration. Major elements have been analyzed with an accuracy of ≤3% and an external precision of ≤3% (2-sigma), whereas minor elements (<1 wt.%) have been determined with an accuracy of ≤6% and an external precision of ≤6% (2-sigma). Replicate analytical results of natural mineral standards are presented in Appendix 1.

Major oxides, trace elements, and platinum-group element (PGE) of whole rocks were analyzed at the SKLODG. Major oxides of samples without mineralization were analyzed with a PANalytical Axios-advance X-ray fluorescence spectrometer (XRF) on fused glass pellets with analytical uncertainties ranging from 1 to 3%. Analytical results of standard materials and replicate analyses are presented in Appendix 1. Major oxides except SiO_2 and selected trace elements (Ni and Cu) of the sulfide ore were determined by inductively coupled plasma atomic emission spectroscopy (ICP-AES). SiO_2 of the sulfide ores were determined by a gravimetric method. Whole-rock S

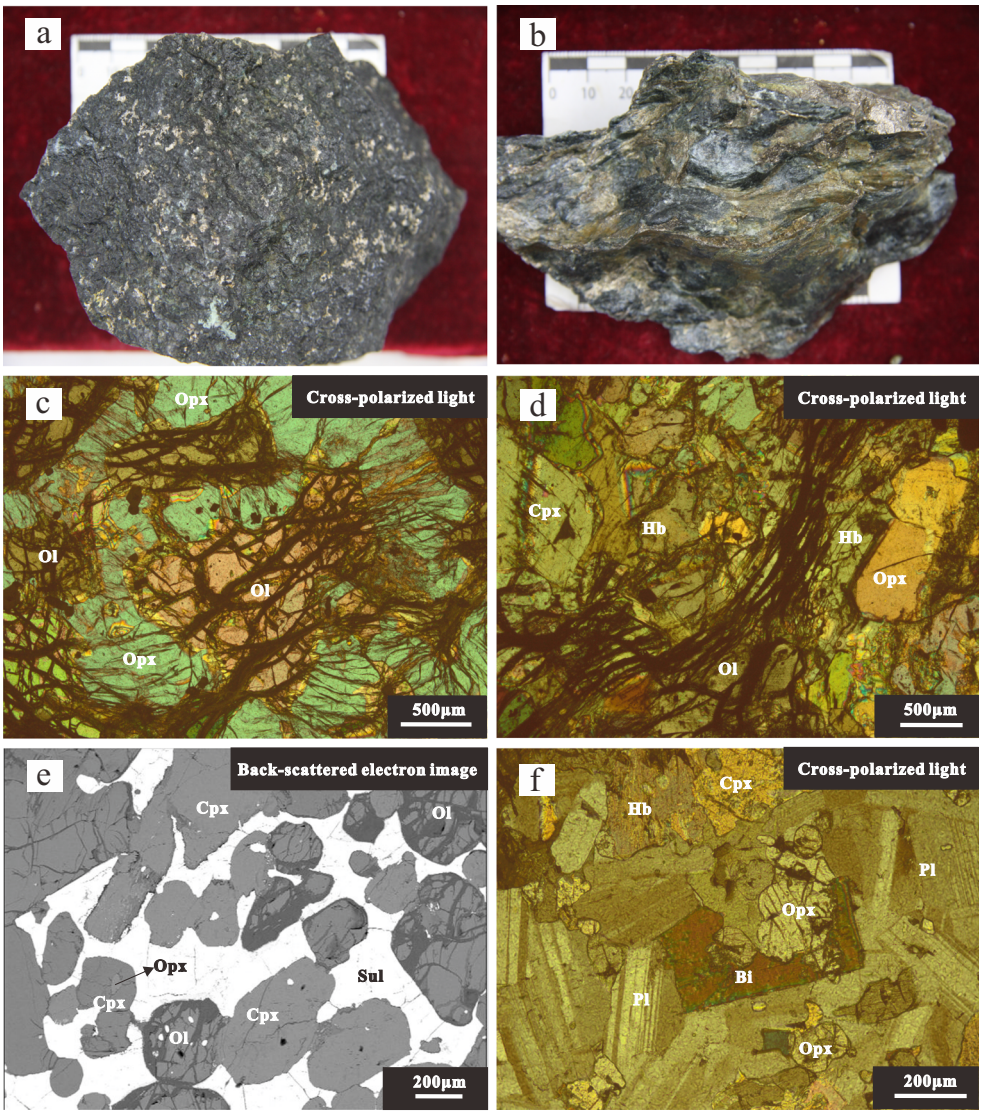

Fig. 3 Photomicrographs of the rocks from the Huangshan intrusion showing **a** the disseminated texture of the sulfide-bearing lower lherzolite, **b** the vein texture of sulfide-bearing lower websterite, **c** olivine crystals enclosed by orthopyroxene in lower lherzolite, **d** the deformed websterite of the middle unit, **e** olivine and clinopyroxene enclosed by sulfide in the lower websterite, and **f** orthopyroxene and clinopyroxene in the basal gabbronorite. *Ol* olivine, *Opx* orthopyroxene, *Cpx* clinopyroxene, *Pl* plagioclase, *Hb* hornblende, *Bi* biotite, *Sul* sulfide

contents were measured by Leco furnace. Trace elements were determined by inductively coupled plasma mass spectrometry (ICP-MS) using the procedure described by Qi et al. (2000). Reference standards, BHVO-2, GBPG-1, and replicate analyses were used to monitor the trace element analyses (Appendix 1). The analytical uncertainty of this procedure is better than 5% for most elements. PGEs were determined by isotope dilution (ID)-ICP-MS using an improved Carius tube technique (Qi et al. 2004, 2007). Five to 10 g of sulfide-poor and 3 to 5 g of sulfide-bearing powdered samples were digested with 35-ml aqua regia in a 75-ml Carius tube placed in a sealed, custom-made, high-pressure, water-filled autoclave. Iridium, Ru, Pt, and Pd were measured by isotope dilution, and ^{194}Pt was used as the internal standard to calculate the abundance of mono-isotopic Rh (Qi et al. 2004). The measured results of PGE for the reference standards WPR-1 and WGB-1 agree with recommended values reported by Qi et al. (2004). Analytical precision and accuracy are generally better than 5%, and the duplicate samples match each other very well (Appendix 1).

Whole-rock sulfur isotopes of sulfide ores were measured on a Finnigan MAT 252 continuous flow isotope ratio mass spectrometry at the Institute of Geochemistry, Chinese Academy of Sciences, with an analytical uncertainty less than 0.2‰ (Appendix 1). Analyses of the GBW04414 S standard yielded a value of −0.063‰ (n = 12). All sulfur isotopic data are reported relative to V-CDT in standard δ notation.

Results

Mineral composition

Olivine grains were analyzed from the lower websterite, lower lherzolite, and websterite of the Huangshan intrusion. The

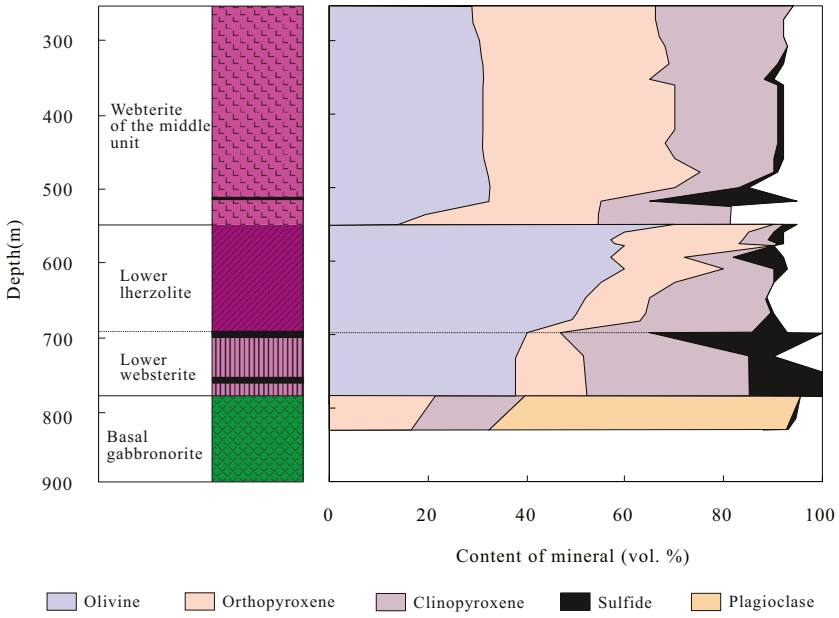

Fig. 4 Stratigraphic variation of mineral contents in drill hole ZK118-7 from the Huangshan intrusion. Contents of hornblende, biotite, Cr-spinel, and loss on ignition (LOI) are not shown in the figure

olivines have forsterite (Fo) values varying from 70.7 to 85.8% and NiO from 0.04 to 0.12 wt.% (Appendix 2). The Fo contents of two olivine grains from the altered websterites near the contact with the lower lherzolites are lower than those of the upper samples. The Fo contents of the lower lherzolites generally decrease with depth (from 85.5 to 82.2%), which are higher than those of lower websterite. From the base to the top of the lower lherzolite, MgO contents gradually increase, whereas FeO contents decrease. The websterites, the lower lherzolites, and the lower websterites have similar enstatite (En) contents of clinopyroxene (En = 42.2–48.2%) and orthopyroxene (En = 80.3–85.6%), which are distinctly higher than those of the clinopyroxene (En = 39.0–39.9%) and orthopyroxene (En = 61.9–62.3%) from the basal gabbronorites (Appendix 3; Fig. 6). The MgO, SiO_2, FeO, and CaO contents display limited variation upward in the lower lherzolites.

Pyrrhotite, pentlandite, and chalcopyrite compositions were determined by electron-microprobe from the sulfide ores in lower lherzolite and lower websterite. The pyrrhotite in the

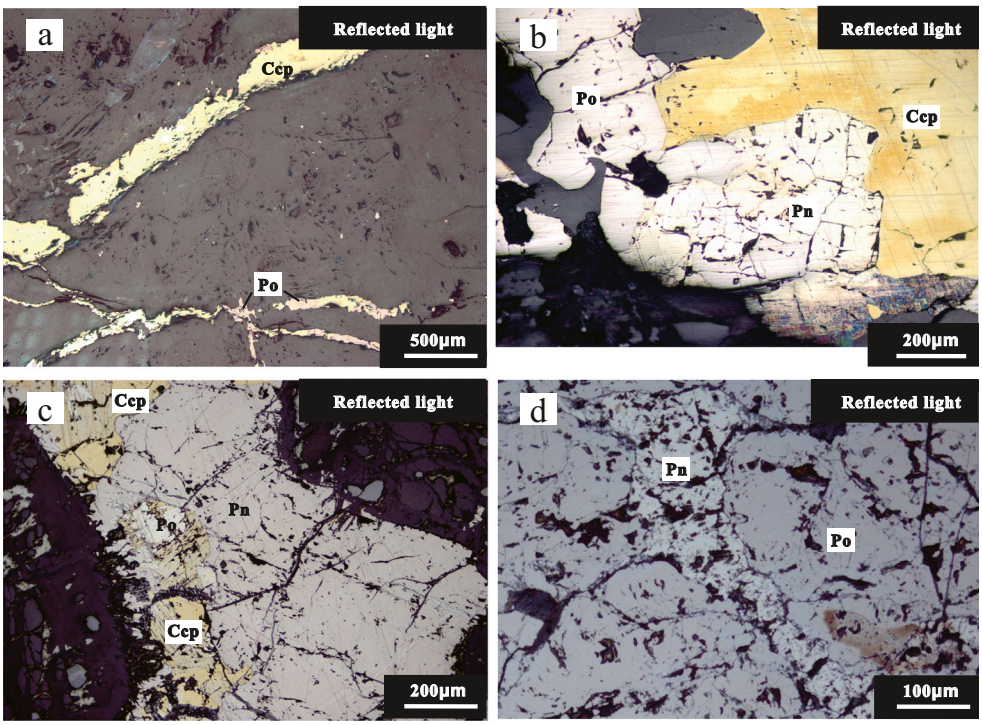

Fig. 5 Reflected light photomicrographs showing vein-textured sulfides in the lower websterite (**a**), net-textured sulfides in the lower websterite (**b**), diseminated sulfides in the lower lherzolite (**c**), and lamellar pentlandite along fractures in pyrrhotite grains (**d**). *Ccp* chalcopyrite, *Pn* pentlandite, *Mt* magnetite, *Po* pyrrhotite, *Ol* olivine

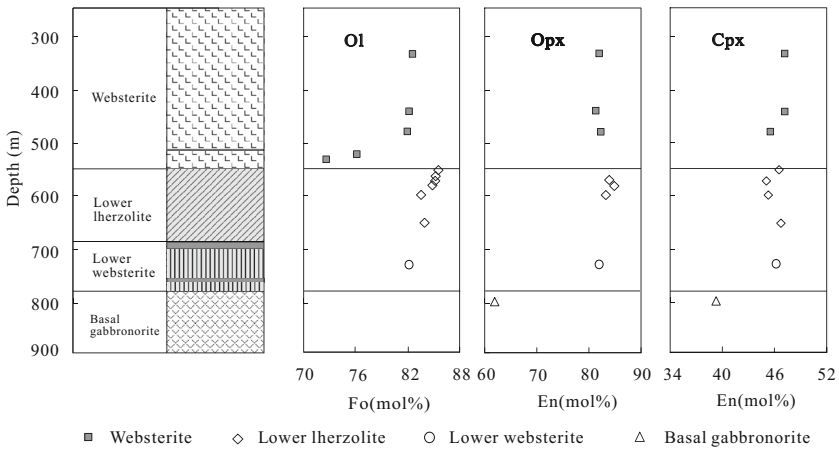

Fig. 6 Stratigraphic variations of average olivine, orthopyroxene, and clinopyroxene compositions in the Huangshan intrusion. Additional mineral composition data are from Song et al. (2013) and Deng et al. (2015)

lower lherzolite contains low S (34.8–37.0%), Ni (0–0.025%), and high Fe (61.5–64.1%) contents, whereas the pyrrhotite in the lower websterite contains higher S (37.2–37.9%) and Ni (0.11–0.85%) and lower Fe contents (60.6–61.1%) than those of the pyrrhotite in the lower websterite. The pentlandite in the lower lherzolite contains high S (32.6–33.4%), Cu (0.10–0.28%), and Co (0.42–0.46%) and low Fe (30.5–31.5%) and Ni (33.7–34.9%), whereas pentlandite in the lower websterite contains lower S (31.8–32.3%), Cu (0.04–0.12%), and Co (0.33–0.36) and higher Fe (31.1–31.6%) and Ni (34.6–35.1%) than those in the lower lherzolite. Moreover, the chalcopyrite in the lower websterite contains lower S, Ni, and Fe contents than those of chalcopyrite in the lower lherzolite (Appendix 4).

Whole-rock geochemistry

Representative major and trace elements contents of the Huangshan rocks are listed in Appendix 5. Because the rocks were altered and contain sulfides, oxide contents have been recalculated to 100% on a volatile-free and sulfide-free basis in the following plots and discussions.

Stratigraphic variations of major oxides of the Huangshan intrusion are illustrated in Fig. 7. The lower lherzolites contain the highest MgO (31.3–33.8 wt.%) and $(Fe_2O_3)_T$ (10.4–12.4 wt.%) and the lowest SiO_2 (37.7–41.6 wt.%) and CaO (0.58–1.82 wt.%; Appendix 5; Fig. 7). The lower websterites have lower MgO (27.5–27.8 wt.%) and $(Fe_2O_3)_T$ (11.3–11.7 wt.%) contents and higher SiO_2 (42.3–43.3 wt.%), and

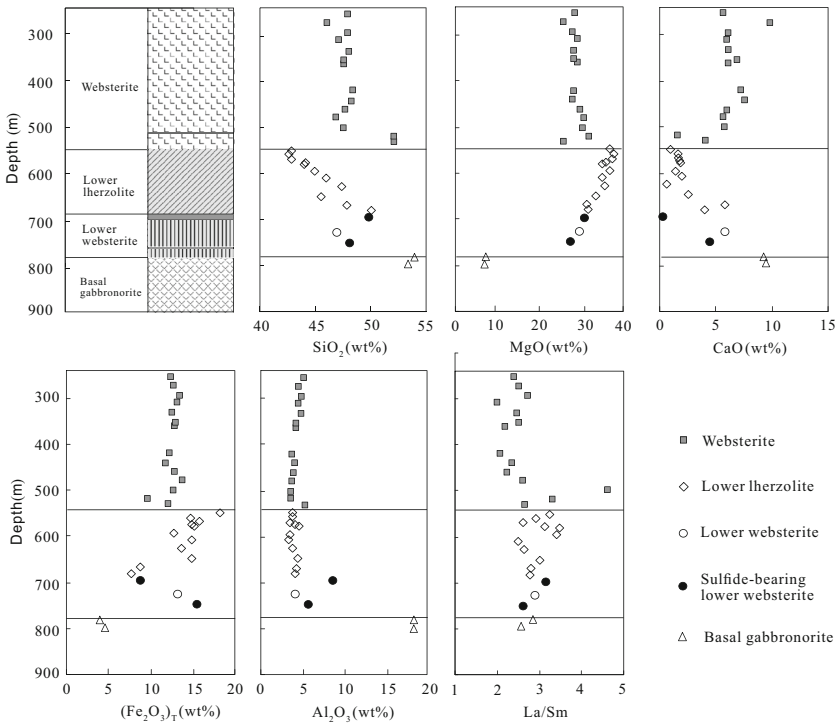

Fig. 7 Chemostratigraphic columns of SiO_2, MgO, CaO, $(Fe_2O_3)_T$, Al_2O_3, and La/Sm through drill hole ZK118-7 in the Huangshan intrusion, showing sharp chemical variations between the websterite, lower lherzolite, and underlying basal gabbronorite. Additional whole-rock data are from Deng et al. (2011)

CaO contents (3.54–5.16 wt.%) than the lower lherzolites (Appendix 5; Fig. 7). In contrast to the lower lherzolites, the websterite has lower MgO (21.7–29.8 wt.%) and $(Fe_2O_3)_T$ contents (9.61–12.2 wt.%), and higher SiO_2 (39.0–46.6 wt.%) and CaO contents (1.46–8.25 wt.%; Fig. 7). Major oxide contents of the lower lherzolite, websterite, and basal gabbronorite are characterized by trends that generally vary across lithological boundaries. The major oxides of the websterite display little variation except for two altered samples near the contact with the lower lherzolites, whereas the SiO_2, MgO, $(Fe_2O_3)_T$, and CaO contents of the lower lherzolites have a large range (Appendix 5; Fig. 7). The SiO_2 and CaO contents of the lower lherzolites decrease with depth, but MgO and $(Fe_2O_3)_T$ contents increase, and Al_2O_3 contents are broadly constant (Fig. 7).

The basal gabbronorite contains relatively high Ba (100–210 ppm), U (0.24–1.46 ppm), La (4.14–9.09 ppm), Nb (1.22–3.23 ppm), and Yb (0.95–2.06 ppm). Compared to the mafic samples, the lower websterite, the lower lherzolite, and the websterite have lower Ba (3.54–84.3 ppm), U (0.11–0.25 ppm), La (1.06–2.78 ppm), Nb (0.28–0.84 ppm), and Yb (0.26–0.67 ppm). Normal Mid-Ocean Ridge Basalts (N-MORB) normalized trace element diagrams show that the Huangshan intrusive rocks are enriched in large ion lithophile elements (e.g., Rb, Th, U, and La) relative to the high field strength elements (e.g., Zr, Hf, and Yb) and exhibit negative Nb-Ta-Ti anomalies (Fig. 8a). The Huangshan rocks are uniformly enriched in LREE relative to HREE ($(La/Yb)_N$ = 2.13–4.03) and have positive to negative Eu anomalies (δEu = 0.72–1.16; Fig. 8b).

Chalcophile element geochemistry and sulfur isotopes

The concentrations of PGE, Cu, Ni, S, and Se in the ultramafic rocks and sulfide ores are presented in Appendix 6. Sulfide contents in the sulfide-mineralized samples were calculated using the procedure of Barnes and Lightfoot (2005): $C_{(100\%sul)} = C_{wr} \times 100/(2.527 \times S + 0.3408 \times Cu + 0.4715 \times Ni)$. $C_{(100\%sul)}$ is the concentration of Pd or Pt in 100% sulfide; C_{wr} is the concentration of the element in the whole rock; and S, Cu, and Ni are the concentrations in wt.% of those elements in the whole rock. It is assumed that the bulk of the sulfides are pyrrhotite, pentlandite, and chalcopyrite. The ΣPGE abundances in the Huangshan ultramafic rocks range from 0.97 to 4.69 ppb with those in the lower lherzolite being similar to those of the websterite, varying from 0.97 to 5.72 ppb. The websterite and lower lherzolite contain Ir (0.018–0.18 ppb), Ru (0.024–0.27 ppb), Rh (0.018–0.41 ppb), Pt (0.38–2.47 ppb), and Pd (0.45–2.64 ppb). However, the sulfide-bearing lower websterite has higher Ir (0.19–1.26 ppb), Ru (0.19–2.01 ppb), Rh (0.3–2.42 ppb), Pt (3.92–21.9 ppb), and Pd (2.53–15.2 ppb) than the websterite and lower lherzolite. Cu/Pd ratios of the silicate rocks are between 8.93×10^4 and 4.05×10^5, much higher than primitive mantle values (7000–10,000; Barnes and Maier 1999).

The mantle-normalized Ni, Cu, and PGE concentrations of the lower lherzolite and the websterite from the Huangshan intrusion are similar (Fig. 9a). The ultramafic rocks have PGE-depleted patterns relative to Ni and Cu and show PPGE (Pt, Pd, and Rh) enrichments relative to IPGE (Ir, Ru; Fig. 9a). On a plot of Pd/Ir vs. Ni/Cu most samples plot in the field of both high-Mg basalts and layered intrusions (Fig. 9b). The Ru/Y and Pd/Y ratios of the mineralized lower lherzolite increase with increasing MgO contents, whereas Ru/Y and Pd/Y ratios of the mineralized lower websterite increase with decreasing MgO (Fig. 10a, b). Though there is an overlap in Ni contents of the sulfide ores in the lower lherzolite and the lower websterite, the Cu contents of the mineralized lower lherzolite are lower than those of the mineralized lower websterite (Fig. 10c). Sulfide ores in the lower lherzolite have Cu/Pd ratios of 2.31×10^5–1.36×10^6 and Ni/Cu of 1.29–8.44 (Zhang et al. 2011; Mao et al. 2014), whereas the sulfide ores in the lower websterite contain higher Cu/Pd (6.65×10^5–2.73×10^6) and lower Ni/Cu (0.22–2.48) relative to those of the sulfide ores in the lower lherzolite (Fig. 10d). The Se/S ratios of the sulfide ores in the Huangshan deposit range from 63.1×10^{-6} to 150×10^{-6}, which falls between the crust ($<50 \times 10^{-6}$) and the mantle ratios (230×10^{-6}–350×10^{-6}; Eckstrand et al. 1989). The $\delta^{34}S$ values of the sulfide ores are

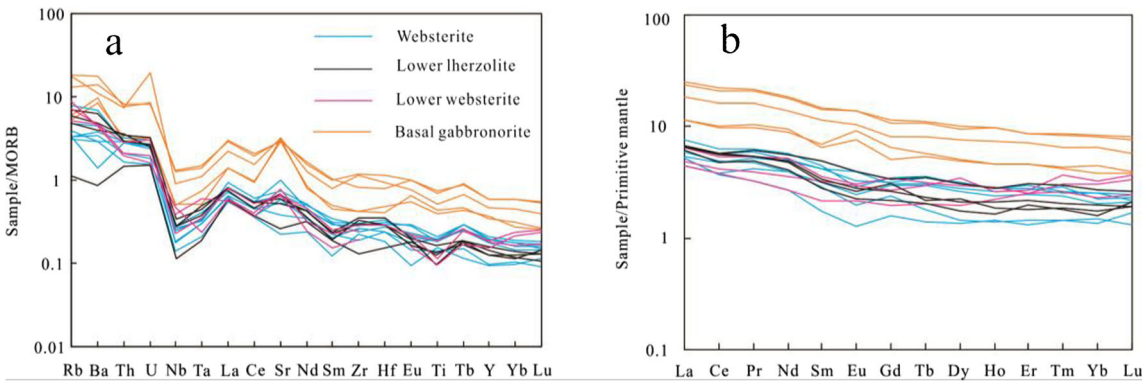

Fig. 8 N-MORB normalized trace element spider diagrams of the Huangshan intrusion. Additional data for the Huangshan intrusion are from Deng et al. (2011). The data for N-MORB and C1 chondrite are taken from Pearce (1982) and Sun and McDonough (1989), respectively

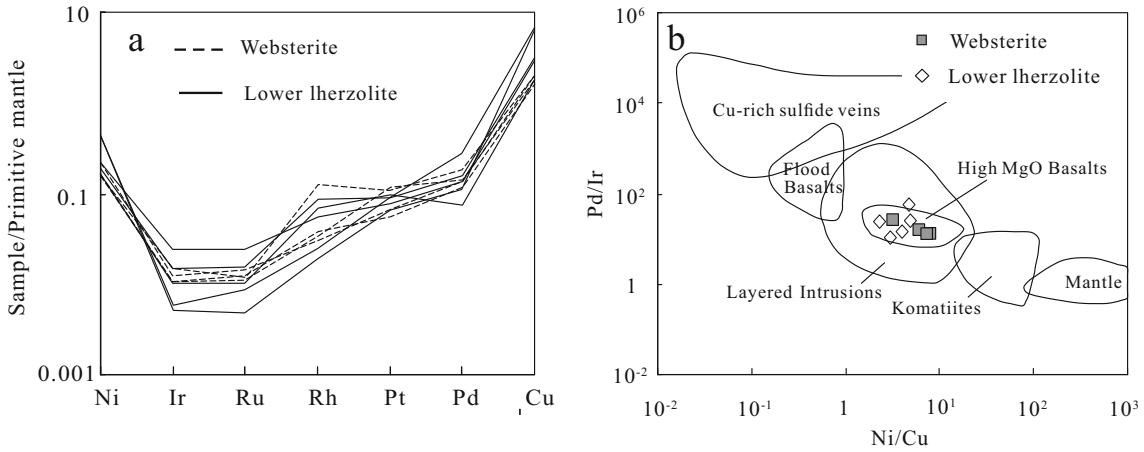

Fig. 9 **a** PGE patterns of the intrusive rocks from the Huangshan intrusion normalized to the primitive mantle (Barnes and Maier 1999); **b** diagram of Pd/Ir vs. Ni/Cu, showing that the Huangshandong intrusive rocks and sulfide ores are associated with basaltic magma (modified after Barnes et al. 1988)

low, varying between 0.63 and 2.42‰ (Appendix 6), similar to typical mantle values (~0 ± 2‰; Ohmoto and Rye 1979).

Discussion

Modeling of olivine compositional variations

Possible influences on olivine composition include magma fractional crystallization, subsolidus reequilibration with interstitial silicate, and trapped sulfide liquids (Barnes 1986; Barnes et al. 2011, 2013; Li et al. 2003, 2007). The contents of Fo and Ni in olivine decrease during fractional crystallization, whereas the compositions of early cumulus olivine can be modified by subsolidus reequilibration with the trapped silicate liquid between the mafic minerals. Diffusion of Fe and Mg within olivine results in olivine with lower Fo contents than the original cumulus minerals. This effect is referred to as "trapped silicate liquid shift" by Barnes (1986) and would account for some of the scatter of the olivine compositions to the right of the model curve for fractional crystallization. Meanwhile, a negative Fo-Ni correlation in olivine from sulfide-bearing rocks is consistent with subsolidus reequilibration of olivine with trapped sulfide liquid (Li et al. 2003, 2007).

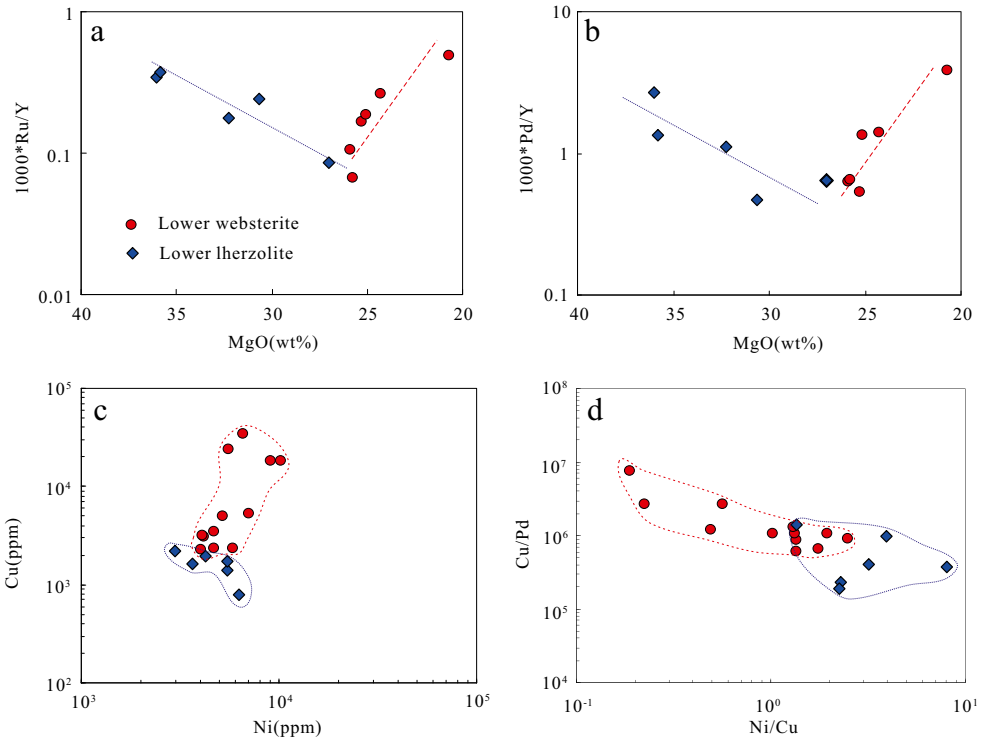

Fig. 10 Whole-rock geochemistry of sulfide ores of the Huangshan Ni-Cu deposit. **a** MgO vs. 1000*Ru/Y, **b** MgO vs. 1000*Pd/Y, **c** tenors of Ni vs. Cu of sulfide mineralization, **d** Ni/Cu ratios vs. Cu/Pd ratios. Data are from this study, Zhang et al. (2011), and Mao et al. (2014). The *blue* and *red straight lines* represent the variation trend of chemical composition of the sulfide from the lower lherzolite and the lower websterite. The *blue* and *red curves* represent the variation fields of chemical composition of the sulfide from the lower lherzolite and the lower websterite, respectively

We have used the PELE (Boudreau and Meurer 1999) program to model the fractional crystallization of a hypothetical magma with compositions similar to high-Mg basalt (Chai and Naldrett 1992) using an initial Ni content of 155 ppm, a partition coefficient of Ni between olivine and magma of 7 at 2.5 kba,r and a FMQ-equivalent oxidation state (Li and Ripley 2005). Initial H_2O content in the magma was assumed to be 3 wt.% based on the occurrence of magmatic hornblende in the Huangshan rocks (Zhou et al. 2004). Modeling results show that olivine, clinopyroxene, and plagioclase crystallized from a parental magma at 1224, 1060, and 1036 °C, respectively. This crystallization sequence is generally in good agreement with petrographic observation. The olivine Fo value and Ni content correlation curve A-B-C is the modeled result of the normal magmatic evolution (Fig. 11). Curve B-D is the trend of olivine Fo value and Ni content when olivine and sulfide crystallized together with the mass ratio of 20:1 after 5.8% of olivine crystallization from the parental magma. Variations of olivine Fo and Ni contents of the lower lherzolites are consistent with the normal crystallization trend, and Ni contents have not been depleted. The Fo and Ni contents of the olivine in websterites are obviously lower than those of the curve A-B-C for normal magmatic evolution (Figs. 6 and 11), indicating that olivine in websterites crystallized from the silicate liquid coexisting with the sulfide liquid.

Magma petrogenesis

The similar primitive mantle normalized patterns of the intrusive rocks from Huangshan intrusion suggest that they were ultimately derived from the same parent magma (Figs. 8 and 9a). The lower websterite, lower lherzolite, websterite, and basal gabbronorite show similar but variable trends, suggesting that they are comagmatic (Zhang et al. 2011; Mao et al. 2014). Using the molar Mg-Fe distribution constant ($K_d = (Fe/Mg)^{Ol}/(Fe/Mg)^{magma}$) of 0.3 ± 0.03 (Roeder and Emslie 1970), the Mg# (atomic Mg/(Fe + Mg)) of the Huangshan parental magmas are estimated to be less than 64 based on the Fo contents of 70.7–85.8% for olivine in the websterite and lower lherzolite. These Mg#s are lower than silicate magma derived from the mantle (68–75%; Wilson 1989). The absence of intermediate-felsic inclusions in the Huangshan intrusion suggests that the relatively low Mg#s were not the result of magma mixing between a basaltic parent magma and intermediate-felsic magma. Previous studies have shown that the La/Sm ratio can be used to trace the assimilation of crustal rocks by a magma (Lassiter and De Paolo 1997; Lightfoot and Keays 2005). The constant Al_2O_3 and La/Sm ratios in the Huangshan intrusion imply that crustal assimilation did not significantly modify the major and trace elements of the intrusive rocks (Zhang et al. 2011; Yang et al. 2012). Thus, the low Mg#s of the Huangshan parent magma are likely the result of variable degrees of fractional crystallization before shallow-level emplacement in the Huangshan magma chamber.

The absence of olivine and the low En values of the pyroxenes indicate that the parental magma of the basal gabbronorite was more evolved with lower Mg# values than the websterite and lower lherzolite. Meanwhile, gradational variation of mineral and whole rock compositions between the lower websterite and lower lherzolite suggests that they formed from the same stage in the evolution of the parent magma (Figs. 6 and 7). The abrupt changes in mineral and major element contents at the contacts between the basal gabbronorite, websterite, and lower lherzolite suggest that they were formed from different intrusive phases (Figs. 4 and 7). This is consistent with the sharp contacts between the basal gabbronorite, lower lherzolite, middle unit, and upper lherzolite. Thus, multiple pulses of magma replenishment in the Huangshan intrusion likely occurred with the first stage forming the upper lherzolite in the eastern part of the intrusion. Following a period of fractionation, the second stage formed the middle unit websterite, norite-gabbro, gabbro, and diorite (Fig. 2). The poikilitic pyroxenes in the websterites have compositions indistinguishable from those in the underlying lower lherzolites and lower websterites, suggesting that they crystallized in situ and were formed by successive pulses of new homogeneous magma passing through the magma conduit. The third stage formed the lower lherzolite and lower websterite. The basal gabbronorite represents the last magmatic intrusion.

That the intrusion formed from multiple pulses of magma is also consistent with reversals in the volume fraction and compositions of both minerals and the whole rock (Figs. 4, 6, and 7).

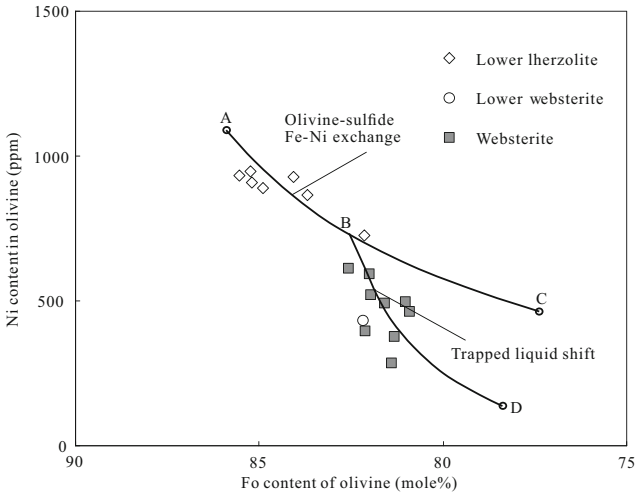

Fig. 11 Model calculation of the variation of nickel content and Fo of the Huangshandong intrusion. For detailed methodology, see Li and Naldrett (1999) and Li et al. (2007). A is the olivine composition in equilibrium with the parental magma. *A-B-C* is the calculated curve modeling the olivine crystallization of the parental magma. *B-D* is the calculated curve modeling 5.8% olivine crystallization from the parental magma, and then olivine and sulfide simultaneously separated (olivine/sulfide = 20/1)

Because mafic silicate minerals (such as olivine and pyroxene) will typically crystallize early in a normal basaltic magma in a closed magmatic system, their accumulation at the base of the intrusion would result in the abundances of these mafic minerals and Mg#s of whole rock decreasing from the bottom up. However, in the Huangshan intrusion, the abundance of olivine and orthopyroxene as well as the Fo contents of olivine increase upward in the lower lherzolite and lower websterite. As shown in Fig. 7, the SiO_2 and CaO contents of the lherzolites and lower websterite generally decrease with decreasing depth, but MgO and $(Fe_2O_3)_T$ contents increase. Thus, the contents and compositions of the mineral and the whole-rock compositions of the lower lherzolite and lower websterite in the Huangshan intrusion are the reverse of those in normally layered intrusions. Similar reversals have been observed in many layered intrusions where they are attributed to a variety of processes that modify fractional crystallization including the intratelluric inhomogeneity of the magma, magma contamination, and trapped liquid shift (Li and Naldrett 1999; Latypov 2003; Latypov et al. 2007; Latypov and Chistyakova 2009). The reversals in the compositions of olivine and the whole-rock compositions in the mafic sills of the Noril'sk deposit were taken as evidence for their formation from an inhomogenous magma (Li et al. 2003; Arndt et al. 2003; Arndt 2005). Crustal contamination may have played an important role in the formation of the whole-rock composition reversal in the Duluth Complex (Tyson and Chang 1984; Severson and Hauck 1990). Reaction of cumulus minerals with an intercumulus melt increasing in abundance towards the base of the intrusion have been used to explain whole-rock composition reversals in the Stillwater Complex (Raedeke and McCallum 1984). The basal reversal in olivine composition in the Voisey's Bay deposit is related in part to the effect of trapped liquid crystallization (Li and Naldrett 1999).

It can be speculated that if a basaltic magma assimilates less silica-rich or more magnesium-rich country rocks with decreasing depth, the mafic cumulate rocks formed by this magma will display reversals of mafic mineral contents and whole-rock compositions. Variations of La/Sm ratios in the lower lherzolite and lower websterite from the Huangshan intrusion are constant, suggesting that whole-rock compositions have not been significantly changed by crustal assimilation. Thus, the reversals of mafic mineral contents and whole-rock compositions are not the result of crustal assimilation. Moreover, the trapped silicate liquid shift can cause the reversal of the olivine compositions if the cumulus olivines are less affected by trapped silicate liquid from the bottom up. The fractional crystallization of silicates and trapped silicate liquid shift can be modeled using the proportions of silicate phases by fractional crystallization (Barnes 1986; Li and Naldrett 1999; Li et al. 2007). The subsolidus reequilibration with the trapped silicate liquid between the mafic minerals would result in Fo contents in olivine cores higher than those of olivine mantle, but olivines from the lower lherzolite in Huangshan intrusion show no evidence of Fo zoning, even in larger grains. Variations in olivine Fo and Ni contents of the lower lherzolite in the Huangshan intrusion are consistent with the model curve for fractional crystallization, but differ from the trend caused by trapped liquid shift (Fig. 11). Additionally, if the reversals in the olivine compositions had been controlled by the trapped liquid shift, olivine compositions of the websterite above the lower lherzolite would have been affected by this process and have displayed similar reversals.

As shown above, the pronounced reversals of abundance and compositions of mineral and whole-rock compositions in the lower lherzolite and lower websterite cannot be the result of crustal assimilation or trapped liquid shift. Rather, it is proposed that the parent magmas underwent variable degrees of fractional crystallization before shallow level emplacement in the Huangshan magma chamber. Olivines with high Fo contents initially crystallized in a deep-seated magma chamber, then were swept up with the advancing magma to the point where the conduit broadened out to form the upper part of the lower lherzolite in the shallow chamber, whereas olivines with lower Fo contents crystallized in the shallow chamber, underplated the upper rocks and formed the lower part of the lower lherzolite and the lower websterite. Thus, the abundance and Fo contents of olivines in the lower lherzolite and lower websterite would increase with decreasing depth. Consequently, the whole-rock composition of those rocks would also be the reverse of those of the mafic cumulate rocks crystallized in normally layered intrusions.

Sulfide saturation

Sulfide saturation is a key process in formation of magmatic Ni-Cu sulfide deposits (Naldrett 1999, 2004; Keays and Lightfoot 2010). Many factors can drive a mafic magma to sulfide saturation, including changes in the chemical composition, temperature, pressure, and oxygen fugacity of the magma (Haughton et al. 1974; Mavrogenes and O'Neill 1999; Li and Ripley 2005; Jugo 2009; Naldrett 2009); however, assimilation of crustal sulfur is believed to be the most important process (Lesher and Keays 2002; Lightfoot and Keays 2005; Keays and Lightfoot 2010). There are several specific mechanisms of sulfur addition in the crustal contamination process (see Barnes and Lightfoot 2005 and references therein). Some authors have argued for bulk assimilation of sulfide-bearing country rocks (e.g., Ripley and Al-Jassar 1987); some envisaged only migration of sulfur gas from heated sediments to the magma (e.g., Ripley 1981; Lesher and Burnham 2001); moreover, others proposed that mafic magmas may selectively assimilate the crustal sulfide and graphite (Naldrett 2004; Thakurta et al. 2008; Zhang et al. 2011; Yang et al. 2012).

The Se/S ratios of mantle-derived rocks are between 230×10^{-6} and 350×10^{-6}, whereas crustal rocks have Se/S ratio $<50 \times 10^{-6}$ (Eckstrand et al. 1989). Thus, sulfide ores

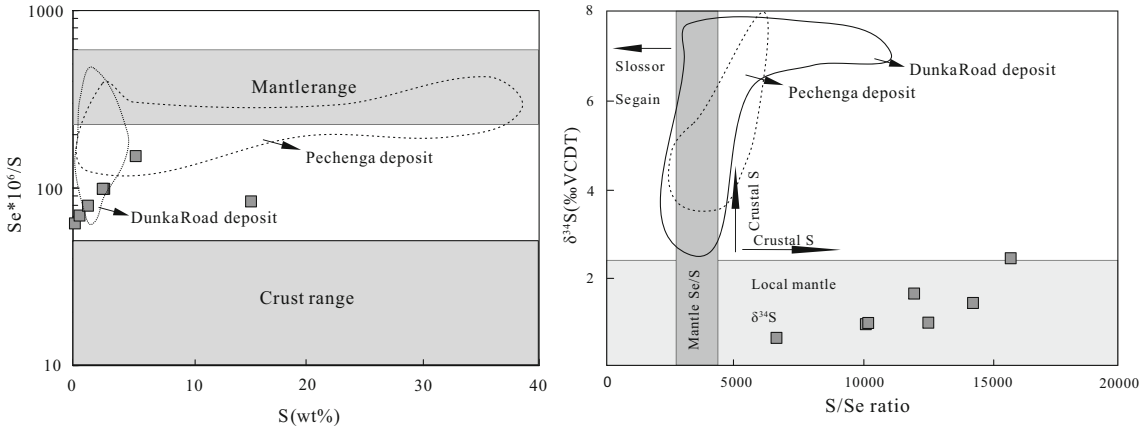

Fig. 12 Plots of **a** Se*10^6/S vs. S and **b** Se*10^6/S vs.δ^{34}S for the Huangshan sulfide ores. The values of the Huangshandong ores are from Deng et al. (2014). The range in Se/S ratio of the mantle and crust is taken from Eckstrand et al. (1989). The data for the Dunka Road and Pechenga deposits are from Theriault and Barnes (1998) and Barnes et al. (2001)

which contain a large contribution of crustal sulfur tend to have low Se/S ratios (Peltonen 1995; Maier et al. 2008; Xie et al. 2014). The Se/S ratios of the Huangshan sulfide ores range from 63.1 to 150 × 10^{-6} (Appendix 6), which is between the ratios of crustal rocks and mantle-derived rocks (Fig. 12a). These values are similar to those of other Ni-Cu sulfide deposits, such as Dunka Road (62.5–476 × 10^{-6}; Theriault and Barnes 1998) and Pechanga (125–386 × 10^{-6}; Barnes et al. 2001), which have been interpreted to have incorporated a crustal sulfur component (Fig. 12a). As shown in Fig. 12b, the S/Se ratios do not plot in the mantle field and the trend of the S/Se is similar to that of crustal S addition, suggesting that there was contamination by crustal sulfur, which could have resulted in extensive sulfide segregation. Because the δ^{34}S value of carbonaceous slates in the Huangshan deposit are 1.75‰ (Wang et al. 1987), similar to those of mantle-derived magma and Huangshan ores (Fig. 12b), so S isotopic composition alone does not constrain the role of external sulfur in the genesis of the Huangshan deposit.

As discussed above, S/Se ratios suggest the presence of a crustal sulfur component in the Huangshan deposit, whereas the La/Sm ratios have not been elevated by crustal assimilation. Because crustal sulfides are less stable than silicates during partial melting or devolatilization of the crust (Lesher and Burnham 2001), they could be selectively incorporated into the mantle-derived magma by assimilation, whereas silicate minerals would be incorporated to a lesser extent owing to their higher melting point. It is suggested that crustal sulfides were selectively assimilated into the silicate magma, thus assimilating more S in preference to other trace elements. The low La/Sm ratios in the crustal sulfides would not significantly affect the La/Sm of the whole rock. The fact that the S/Se ratios would be more sensitive to crustal assimilation than La/Sm suggests that in the Huangshan deposit, contamination was more likely due to the selective assimilation of crustal sulfides. This process is analogous to the crustal contamination model proposed for the Voisey's Bay, Duke Island, and Qingbulake deposits (Lightfoot and Naldrett 1999; Thakurta et al. 2008; Yang et al. 2012).

Origin of sulfide mineralization

The largest ore body in the Huangshan deposit (P30) is composed of sulfide mineralization in the lower lherzolite and the lower websterite. The gradual contact between the lower lherzolite and the lower websterite indicates that they were formed from a single pulse of magma. Calculated sulfide/silicate ratios for the Huangshan intrusion are significantly lower than actual sulfide abundances in the ore bodies, suggesting transportation of immiscible sulfide droplets from depth (Mao et al. 2014; Zhang et al. 2011). Additionally, Sr-Nd isotopic values of the intrusive rocks and S/Se ratios of the sulfide ores are consistent with crustal contamination at depth as the wall rocks to the deposit are barren of sulfide (Zhang et al. 2011). The sulfide ores in the lower lherzolite are mainly disseminated sulfides (Fig. 3a), suggesting that sulfides were accumulated from the staging chamber coeval with the emplacement of silicate minerals. In contrast, the sulfide veins in the lower websterite have sharp contacts with the host rocks and contain pyrrhotite, chalcopyrite, and pentlandite, which are similar to the magmatic assemblage. Moreover, there are no low-temperature hydrothermal minerals (i.e., quartz, calcite, pyrite) in these sulfide veins, which is not consistent with the deformed and hydrothermally remobilized Sarah's Find Ni-Cu-(PGE) in western Australia (Vaillant et al. 2016), so a metasomatic infiltration or postmagmatic modification model is unlikely. Thus, the vein-textured sulfides in the lower websterite suggest that some sulfide melts were intruded after the emplacement of the cumulate silicates (Figs. 3 and 5). The Huangshan intrusion (284.5–283.8 Ma; Gu et al. 2006; Qin

et al. 2011) was likely emplaced as a synkinematic sheeted intrusion by injection of several magma batches within kilometer-scale tension gashes generated by Permian dextral shearing (300–283.7 Ma; Chen et al. 2005; Branquet et al. 2012). The minerals in some websterites and the lower websterite have been deformed by the regional shearing, whereas the minerals in the sulfide zones of the lower websterite have not (Figs. 3 and 5). This implies that the sulfides were intruded into the lower websterite after the emplacement of cumulates and the regional deformation. Though the lower websterite and lower lherzolite were formed by the same magma pulse, the sulfides in the lower websterite were formed slightly later than those in the lower lherzolite. Moreover, the compositional differences between the sulfide minerals in the lower lherzolite and lower websterite indicate that two pulses of sulfide melts were required to form the sulfide ores.

The sulfide ores in the lower websterite have higher Cu contents and Cu/Pd ratios but lower Ni/Cu ratios than in the lower lherzolite (Fig. 10d). On plots of Ru/Y and Pd/Y ratios against MgO (Fig. 10a, b), the sulfides in the lower lherzolite display different trends from the sulfides in the lower websterite, supporting the interpretation that the sulfides in these two units likely formed from sulfide melts with distinct compositions. Because the geochemical signatures of the Huangshan intrusion are similar to those of island-arc magmas, we assume that the Huangshan intrusion had a source similar to a PGE-undepleted island-arc basaltic magma, with 4 ppb Pd, 0.07 ppb Ir, and 85 ppm Cu (Barnes et al. 1993; Kelemen et al. 2004). The partition coefficients of Cu, Ir, and Pd between sulfide and silicate magma were assumed to be 1000, 30,000, and 40,000, respectively (Peach et al. 1990; Fleet et al. 1993; Crocket et al. 1997). Using the mass balance equation proposed by Campbell and Naldrett (1979), the sulfides in the lower lherzolite and the lower websterite probably segregated from the same parent magma which underwent 0.015% early sulfide removal under R factors of 100 to 2000 (Fig. 13a, where the R factor is the mass ratio of silicate magma to sulfide melt).

Experimental studies have shown that Os, Ir, Ru, and Rh are compatible into monosulfide solid solution (MSS), whereas Pt, Pd, Au, and Cu are incompatible in the MSS structure and tend to concentrate in the residual sulfide liquid (Fleet et al. 1993; Li et al. 1996; Barnes et al. 1997; Mungall et al. 2005). Consequently, Pd/Ir and Ni/Ir ratios increase as the sulfides accumulate the MSS. On the other hand, the sulfide liquid/silicate melt partitioning coefficients of PGEs are similar, but are all much higher than that of Ni (Francis 1990; Fleet et al. 1993). If the sulfide liquids reacted with a large volume of S-unsaturated magma, Pd/Ir will vary very little and the Ni/Ir ratio will decrease. The limited variation of the Pd/Ir ratios with decreasing Ni/Ir ratios of the sulfides in the lower lherzolite (Fig. 13b) suggests that the sulfide liquids experienced upgrading of PGE by reaction with successive pulses of primary S-unsaturated magma, rather than fractional crystallization of MSS (Lesher and Burnham 2001). This reaction process would have resulted in elevated R factors and enrichment of metal elements (Fig. 13b; Li et al. 2000, 2003; Song et al. 2008). In contrast, the positive correlations between Ni/Ir and Pd/Ir of the sulfide in the lower websterite suggest a role for MSS fractional crystallization and explain the different characteristics of the two generations of sulfides (Fig. 13b).

Implications for dynamic ore-forming processes

Many important magmatic Ni-Cu sulfide deposits have been found in small intrusions which have been interpreted to have formed by emplacement of multiple magma pulses (such as Jinchuan, Heishan, Kabanga, Eagle and East Eagle, Uitkomst, and Aguablanca; Li et al. 2002, 2012; Song et al. 2003, 2012; Tornos et al. 2006; Song and Li 2009; Maier et al. 2010; Ding et al. 2010; Xie et al. 2012; Xie et al. 2014; Chen et al. 2013). The mass-balance calculations indicate that the host intrusions cannot supply enough Ni to form magmatic sulfide deposits, so these ore-bearing intrusions likely represent a dynamic magma conduit, which scavenge sulfide droplets and crystal mushes from the staging magma chamber. Zhang et al. (2011) inferred that >40% of the magmas involved in the formation of the Huangshan intrusion ascended to form dikes or erupt on the surface. Additionally, the Huangshan intrusion contains a large proportion (>85%) of ultramafic rocks (i.e., websterite, lower lherzolite, and lower websterite) and reversals in olivine

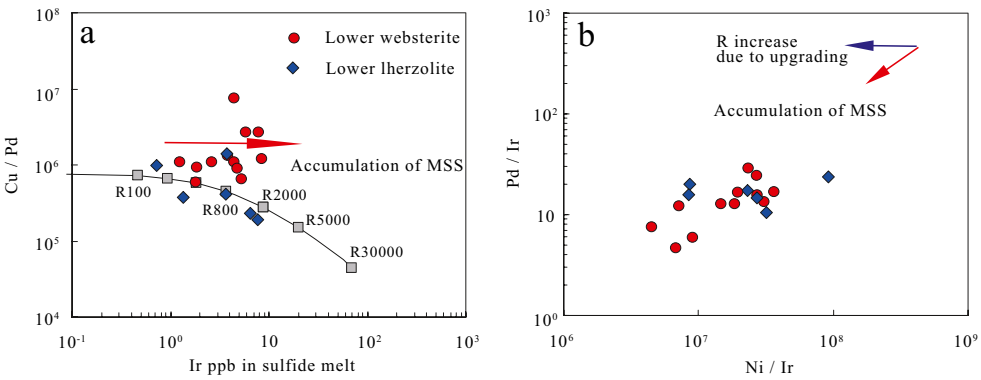

Fig. 13 Plots of the Huangshan sulfides showing **a** Pd/Ir vs. Ni/Ir in sulfide melt; **b** modeling of R factors with Ir and Cu/Pd tenors of sulfide mineralization. Data for the Huangshan deposit are from this study, Zhang et al. (2011), and Mao et al. (2014)

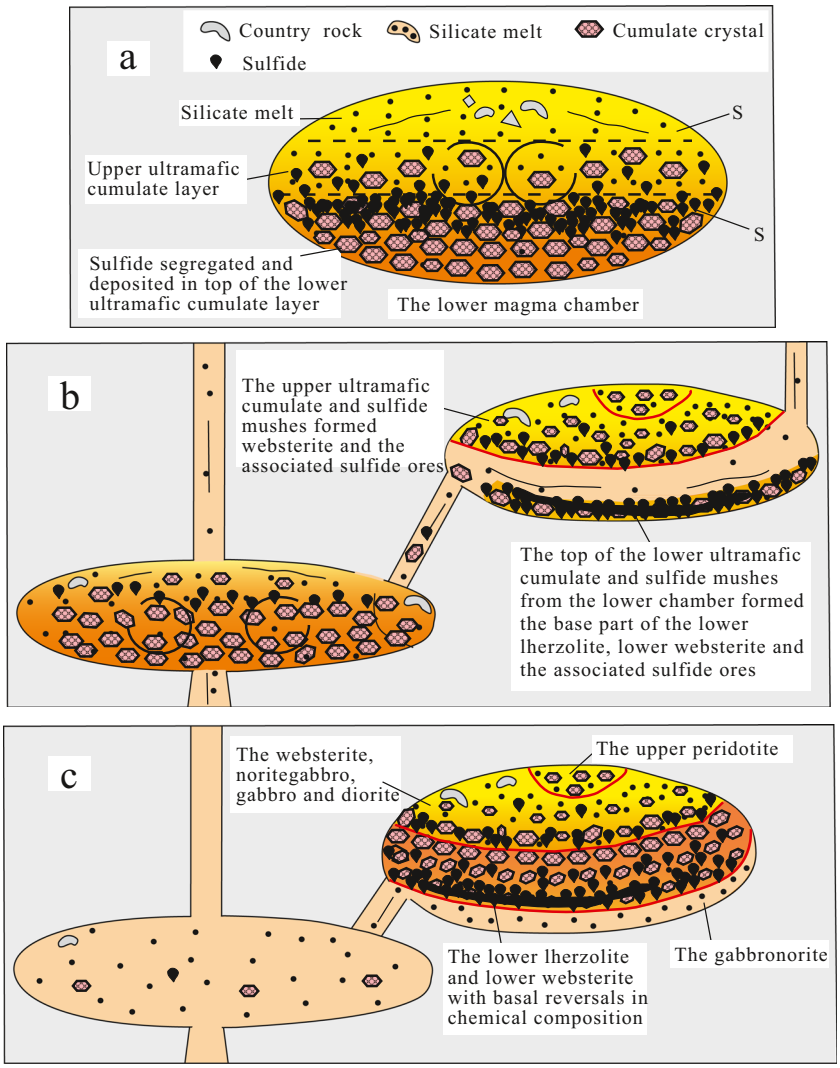

Fig. 14 Genetic model for the Huangshan deposit. See text for detailed discussion

composition and major oxides in the lower lherzolite (Figs. 6 and 7), consistent with intrusion as part of a conduit system through which at least four pulses of magma passed.

The genetic model of the Huangshan deposit is illustrated in Fig. 14. An initial pulse of magma rose to a lower chamber and fractionated to form ultramafic cumulates and silicate melts. After ~5.8% crystallization, the magma reached sulfide saturation because of assimilation of crustal sulfur. The sulfide melts settled on the mafic cumulates that formed earlier in the middle part of the lower chamber (Fig. 14a). The upper ultramafic cumulates and the silicate melts were squeezed into the shallow magma chamber at the point where the magma conduit broadened out and formed the websterite, noritegabbro, gabbro, and diorite. In the meantime, the sulfide in these mushes settled at the base of the websterite and formed a layer of sulfide ore (P31 ore body). With the entry of a fresh magma pulse into the lower chamber, the top of the lower ultramafic cumulates with low Fo olivines were forced upward to form the basal part of the lherzolite in the shallow chamber under the websterite (Fig. 14b). The unfractionated sulfides in the lower chamber coexisting with the top of the lower ultramafic cumulates were swept up with the advancing magma, intruded into the tension gashes generated by Permian dextral shearing, precipitated at the base of the lower lherzolite and lower websterite and formed the largest disseminated and net-textured sulfide ore bodies in the deposit (P30 ore body). Fractionated sulfide melts in the lower chamber were squeezed into the upper magma chamber and emplaced into fissures in the lower websterite forming the vein-textured sulfides. Then, the bottom of the lower ultramafic cumulates with high Fo olivines in the lower chamber were forced upward to form the top part of the lower lherzolite and the lower websterite in the shallow chamber under the websterite (Fig. 14c). When continuous magmas flowed through the mafic cumulates and the coexisting sulfide, they interacted with the sulfides and lost some of their Ni and Cu, enriching these sulfides in this process. Finally, the last pulse of magma was emplaced in the shallow chamber under the lherzolite forming the basal gabbronorite.

Conclusions

The lithological and geochemical characteristics of the Huangshan intrusive rocks suggest that the intrusion was formed from multiple pulses of magma. Reversals in olivine Fo contents and whole-rock compositions of the lower lherzolite and lower websterite were likely the result of inhomogeneity of olivines from the lower chamber. Assimilation of crustal sulfur played a critical role in generating sulfide saturation in the parental magma. The positive correlations between Ni/Ir and Pd/Ir of the vein-textured sulfides in the lower websterite were likely generated by fractionated sulfides transported with a new pulse of magma. In contrast, the limited variation of the Pd/Ir with decreasing Ni/Ir of the disseminated sulfides in the lower lherzolite resulted from a reaction between the sulfides and new pulses of S-undersaturated magmas.

Acknowledgements We thank the management of No. 6 Geological Party, Xinjiang Bureau of Geology and Mineral Resources, for help during our field work. This work was supported by the China Academy of Science "Light of West China" Program, the National Natural Science Foundation of China (Grant Nos. 41630316, 41303031, and 41672069), the Chinese National Science and Technology Program during the 12th Five-year Plan Period (2011BAB06B01), and Open Funds from the State Key Laboratory of Ore Deposit Geochemistry, Institute of Geochemistry, Chinese Academy of Sciences (201102).

References

Arndt NT, Czamanske G, Walker RJ, Chauvel C, Fedorenko V (2003) Geochemistry and origin the intrusive hosts of the Noril'sk-Talnakh Cu–Ni–PGE sulfide deposits. Econ Geol 98:495–515

Arndt NT (2005) The conduits of magmatic ore deposits. In: Exploration for platinum-group element deposits (JE Mungall, ed). Mineral Assoc Canada, Short Course Ser 35:181–201

Barnes SJ (1986) The effect of trapped liquid crystallization on cumulus mineral compositions in layered intrusions. Contrib Mineral Petrol 93:524–531

Barnes SJ, Couture JF, Sawyer EW, Bouchaib C (1993) Nickel-copper occurrences in the Belleterre-Angliers belt of the Pontiac Subprovince and the use of Cu-Pd ratios in interpreting platinum-group element distributions. Econ Geol 88:1402–1419

Barnes SJ, Zientek ML, Severson MJ (1997) Ni, Cu, Au, and platinum-group element contents of sulphides associated with intraplate magmatism: a synthesis. Can J Earth Sci 34:337–351

Barnes SJ, Maier WD (1999) The fractionation of Ni, Cu, and the noble metals in silicate and sulfide liquids. In: Keays RR, Lesher CM, Lightfoot PC, Farrow CEG (eds) Dynamic processes in magmatic ore deposits and their application to mineral exploration, Geological Association of Canada, Short Course Notes, vol 13, pp. 69–106

Barnes SJ, Melezhik VA, Sokolov SV (2001) The composition and mode of formation of the Pechenga nickel deposits, Kola Peninsula, Northwestern Russia. Can Mineral 39:447–471

Barnes SJ, Lightfoot PC (2005) Formation of magmatic nickel sulfide group ore deposits and processes affecting their copper and platinum-group element contents. Economic Geology 100th Anniversary Volume: 179–213

Barnes SJ, Boyd R, Korneliussen A, Nilsson LP, Often M, Pedersen RB, Robins B (1988) The use of mantle normalisation and metal ratios in discriminating between the effects of partial melting, crystal fractionation and sulphide segregation on platinum group metals, gold, nickel and copper: examples from Norway. In: Prichard HM, Potts PJ, Bowles JFW, Cribbs SJ (eds) GeoPlatinum-87. Elsevier, London, pp 113–143

Barnes SJ, Godel BM, Locmelis M, Fiorentini ML, Ryan CG (2011) Extremely Ni-rich Fe-Ni sulfide assemblages in komatiitic dunite at Betheno, Western Australia: results from synchrotron X-ray fluorescence mapping. Aust J Earth Sci 58:691–709

Barnes SJ, Godel B, Gürer D, Brenan JM, Robertson J, Paterson D (2013) Sulfide-olivine Fe-Ni exchange and the origin of anomalously Ni rich magmatic sulfides. Econ Geol 108:1971–1982

BGMX (Bureau of Geology and Mineral Resources of Xinjiang Uygur Autonomous Region) (1993) Regional geology of Xinjiang Uygur autonomous region. Geological Publishing House, Beijing, pp. 1–841 (in Chinese with English abstract)

Boudreau AE, Meurer WP (1999) Chromatographic separation of the platinum-group elements, gold, base metals and sulfur during degassing of a compacting and solidifying igneous crystal pile. Contrib Mineral Petrol 134:174–185

Branquet Y, Gumiaux C, Sizaret S, Barbanson L, Wang B, Cluzel D, Li GR, Delaunay A (2012) Synkinematic mafic/ultramafic sheeted intrusions: emplacement mechanism and strain restoration of the Permian Huangshan Ni-Cu ore belt (eastern Tianshan, NW China). J Asian Earth Sci 56:240–257

Campbell IH, Naldrett AJ (1979) The influence of silicate: sulfide ratios on the geochemistry of magmatic sulfides. Econ Geol 74:1503–1506

Chai G, Naldrett AJ (1992) The Jinchuan ultramafic intrusion: cumulate of a high-Mg basaltic magma. J Petrol 33:277–303

Chen LM, Song XY, Keays RR, Tian YL, Wang YS, Deng YF, Xiao JF (2013) Segregation and fractionation of magmatic Ni-Cu-PGE sulfides in the western Jinchuan intrusion, northwestern China: insights from platinum group element geochemistry. Econ Geol 108:1793–1811

Chen W, Sun S, Zhang Y, Xiao WJ, Wang YT, Wang QL, Jiang LF, Yang JT (2005) $^{40}Ar/^{39}Ar$ geochronology of the Qiugemingtashi-Huangshan ductile shear zone in East Tianshan, Xinjiang, NW China. Acta Geol Sin 79:790–804 (in Chinese with English abstract)

Crocket JH, Fleet ME, Stone WE (1997) Implications of composition for experimental partitioning of platinum-group elements and gold between sulfide liquid and basalt melt: the significance of nickel. Geochim Cosmochim Acta 61:4139–4149

Deng YF, Song XY, Chen LM, Cheng SL, Zhang XL, Li J (2011) Features of the mantle source of the Huangshanxi Ni-Cu sulfide-bearing mafic-ultramafic intrusion, eastern Tianshan. Acta Petrol Sin 27:3640–3652 (in Chinese with English abstract)

Deng YF, Song XY, Chen LM, Zhou TF, Pirajno F, Yuan F, Xie W, Zhang DY (2014) Geochemistry of the Huangshandong Ni-Cu deposit in northwestern China: implications for the formation of magmatic sulfide mineralization in orogenic belts. Ore Geol Rev 56:181–198

Deng YF, Song XY, Hollings P, Zhou T, Yuan F, Chen LM, Zhang D (2015) Role of asthenosphere and lithosphere in the genesis of the early Permian Huangshan mafic-ultramafic intrusion in the Northern Tianshan, NW China. Lithos 227:241–254

Ding X, Li CS, Ripley EM, Rossell D, Kamo S (2010) The Eagle and East Eagle sulfide ore-bearing maficultramafic intrusions in the Midcontinent Rift System, upper Michigan: geochronology and petrologic evolution. Geochem Geophys Geosyst 11(3):Q03003. doi:10.1029/2009GC002546

Eckstrand O, Grinenko L, Krouse H, Paktunc A, Schwann P, Scoates R (1989) Preliminary data on sulphur isotopes and Se/S ratios, and the source of sulphur inmagmatic sulphides from the Fox River Sill, Molson Dykes and Thompson nickel deposits, northern

Manitoba1. Current Research Part: C, Geological Survey of Canada, Paper 89-1C: 235–242

Fleet ME, Chryssoulis SL, Stone WE, Weisener CG (1993) Partitioning of platinum-group elements and Au in the Fe–Ni–Cu–S system: experiments on the fractional crystallization of sulfide melt. Contrib Mineral Petrol 115:36–44

Francis RD (1990) Sulfide globules in mid-ocean ridge basalts (MORB), and the effect of oxygen abundance in Fe-S-O liquids on the ability of those liquids to partition metals from MORB and komatiitic magmas. Chem Geol 85:199–213

Gao JF, Zhou MF (2012) Generation and evolution of siliceous high magnesium basaltic magmas in the formation of the Permian Huangshandong intrusion (Xinjiang, NW China). Lithos 162-163: 128–139

Gao JF, Zhou MF, Lightfoot PC, Wang CY, Qi L, Sun M (2013) Sulfide saturation and magma emplacement in the formation of the Permian Huangshandong Ni-Cu sulfide deposit, Xinjiang, northwestern China. Econ Geol 108:1833–1848

Gu LX, Zhang ZZ, Wu CZ, Wang YX, Tang JH, Wang CS, Xi AH, Zheng YC (2006) Some problems on granitesand vertical growth of the continental crust in the eastern Tianshan Mountains, NW China. Acta Petrol Sin 22:1103–1120 (in Chinese with English abstract)

Haughton D, Roeder P, Skinner B (1974) Solubility of sulfur in mafic magmas. Econ Geol 69(4):451–467

Jahn BM, Wu FY, Chen B (2000) Massive granitoid generation in Central Asia: Nd isotope evidence and implication for continental growth in the Phanerozoic. Episodes 23:82–92

Jahn BM (2004) The Central Asian Orogenic Belt and growth of the continental crust in the Phanerozoic. Geol Soc, London, Spec Publ 226:73–100

Jiao JG, Tang ZL, Qian ZZ, Sun T, Duan J, Jiang C (2012) Genesis and metallogenic process of Tulargen large scale Cu-Ni sulfide deposit in eastern Tianshan area, Xinjiang. Acta Petrol Sin 28:3772–3786 (in Chinese with English abstract)

Jugo P (2009) Sulfur content at sulfide saturation in oxidized magmas. Geology 37:415–418

Keays RR, Lightfoot PC (2010) Crustal sulfur is required to form magmatic Ni-Cu sulfide deposits: evidence from chalcophile element signatures of Siberian and Deccan trap basalts. Mineral Deposita 45:241–257

Kelemen PB, Hanghøj K, Greene AR (2004) One view of the geochemistry of subduction-related magmatic arcs, with an emphasis on primitive andesite and lower crust. In: Rudnick RL (ed) Treatise on geochemistry, the crust. Elsevier, Amsterdam, pp. 593–659

Lassiter JC, De Paolo DJ (1997) Plume/lithosphere interaction in the generation of continental and oceanic flood basalts: chemical and isotope constraints. Geophys Monogr 100:335–355

Latypov RM (2003) The origin of marginal compositional reversals in basic-ultrabasic sills and layered intrusions by Soret fractionation. J Petrol 44:1579–1618

Latypov RM, Chistyakova SY, Alapieti TT (2007) Revisiting problem of chilled margins associated with marginal reversals in mafic-ultramafic intrusive bodies. Lithos 99:178–206

Latypov RM, Chistyakova SY (2009) Phase equilibria testing of a multiple pulse mechanism for origin of mafic-ultramafic intrusions: a case example of the Shiant Isles Main Sill, NW Scotland. Geol Mag 146:851–875

Lesher CM, Burnham OM (2001) Multicomponent elemental and isotopic mixing in Ni-Cu- (PGE) ores at Kambalda. Western Aust: Can Mineral 39:421–446

Lesher CM, Keays RR (2002) Komatiite-associated Ni-Cu-(PGE) deposits: geology, mineralogy, geochemistry and genesis. In: Cabri L (ed) The geology, geochemistry, mineralogy and beneficiation of the platinum-group elements, Canadian Institute of Mining, Metallurgy and Petroleum, Special Volume 54, pp. 579–617

Li CS, Barnes SJ, Makovicky E, Rose-Hansen J, Makovicky M (1996) Partitioning of nickel, copper, iridium, rhenium, platinum, and palladium between monosulfide solid solution and sulfide liquid: effects of composition and temperature. Geochim Cosmochim Acta 60:1231–1238

Li CS, Naldrett AJ (1999) Geology and petrology of the Voisey's Bay intrusion: reaction of olivine with sulfide and silicate liquids. Lithos 47:1–31

Li C, Lightfoot PC, Amelin Y, Naldrett AJ (2000) Contrasting petrological and geochemical relationships in the Voisey's Bay and Mushuau intrusions, Labrador, Canada: implications for ore genesis. Econ Geol 95:771–799

Li C, Ripley EM, Maier WD, Gomwe TES (2002) Olivine and sulfur isotopic compositions of the Uitkomst Ni–Cu sulfide ore-bearing complex, South Africa: evidence for sulfur contamination and multiple magma emplacements. Chem Geol 188:149–159

Li CS, Ripley EM, Naldrett AJ (2003) Compositional variations of olivine and sulfur isotopes in the Noril'sk and Talnakh intrusions, Siberia: implications for oreforming processes in dynamic magma conduits. Econ Geol 98:69–86

Li CS, Ripley EM (2005) Empirical equations to predict the sulfur content of mafic magmas at sulfide saturation and applications to magmatic sulfide deposits. Mineral Deposita 40:218–230

Li CS, Naldrett AJ, Ripley EM (2007) Controls on the Fo and Ni contents of olivine in sulfide-bearing mafic/ultramafic intrusions: principles, modeling, and examples from Voisey's Bay. Earth Sci Front 14:177–185

Li CS, Zhang MJ, Fu PE, Qian ZZ, Hu PQ, Ripley EM (2012) The Kalatongke magmatic Ni–Cu deposits in the Central Asian Orogenic Belt, NW China: product of slab window magmatism? Mineral Deposita 47:51–67

Li DH, Bao X, Zhang B, Han Z, Lan G, Zheng Z et al. (1989) Investigation of geology, geophisics and geochemistry of the Huangshan-Cu-Ni metallogenic belt for mineral exploration. Unpubl Report, National 305 Project Office in Xinjiang. 1–418 (in Chinese)

Li XH, Su L, Chung SL, Li XZ, Liu Y, Song B, Liu DY (2005) Formaton of the Jinchuan ultramafic intrusion and the world's third largest Ni-Cu sulfide deposit: associated with the similar to 825 Ma South China mantle plume. Geochem Geophys Geosestems 6(11), Q1104, dio:10.1029/2005GC001006

Lightfoot PC, Naldrett AJ (1999) Geological and geochemical relationships in the Voisey's Bay intrusion, Nain Plutonic Suite, Labrador, Canada. Geol Assoc Can Short Course Notes 13:1–30

Lightfoot PC, Keays RR (2005) Siderophile and chalcophile metal variations in flood basalts from the Siberian Trap, Noril'sk Region: implications for the origin of the Ni-Cu-PGE sulfide ores. Econ Geol 100:439–462

Liu DQ, Tang YL, Zhou RH (2005) Copper deposits and nickel deposits in Xinjiang. Geological Publishing House, Beijing 360 p. (in Chinese with English abstract)

Maier WD, Barnes SJ, Chinyepi G, Barton JJ, Eglington B, Setshedi T (2008) The composition of magmatic Ni-Cu-(PGE) sulfide deposits in the Tati and Selebi-Phikwe belts of eastern Botswana. Mineral Deposita 43:37–60

Maier WD, Barnes SJ, Sarkar A, Ripley EM, Li CS, Livesey T (2010) The Kabanga Ni sulfide deposit, Tanzania: I. Geology, petrography, silicate rock geochemistry, and sulfur and oxygen isotopes. Mineral Deposita 45:419–441

Mao JW, Pirajno F, Zhang ZH, Chai FM, Wu H, Chen SP, Chen LS, Yang JM, Zhang CQ (2008) A review of the Cu-Ni sulphide deposits in the Chinese Tianshan and Altay orogens (Xinjiang Autonomous Region, NW China): principal characteristics and ore-forming processes. J Asian Earth Sci 32:184–203

Mao YJ (2014) Petrogenesis and ore genesis of the muti-stage mafic-ultramafic intrusions in the Huangshan Ni-Cu camp, Eastern

Tianshan, southern Central Asian Orogenic Belt. Ph.D. Dessertation. Beijing: University of Chinese Academy of Sciences, 178 p. (in Chinese with English abstract)

Mao YJ, Qin KZ, Li CS, Xue SC, Ripley EM (2014) Petrogenesis and ore genesis of the Permian Huangshanxi sulfide ore-bearing mafic-ultramafic intrusion in the Central Asian Orogenic Belt, western China. Lithos 200-201:111–125

Mao YJ, Qin KZ, Li CS, Tang DM (2015) A modified genetic model for the Huangshandong magmatic sulfide deposit in the Central Asian Orogenic Belt, Xinjiang, western China. Mineral Deposita 50:65–82

Mavrogenes JA, O'Neill HSC (1999) The relative effects of pressure, temperature and oxygen fugacity on the solubility of sulfide in mafic magmas. Geochim Cosmochim Acta 63:1173–1180

Mungall JE, Andrews DRA, Cabri LJ, Sylvester PJ, Tubrett M (2005) Partitioning of Cu, Ni, Au, and platinum-group elements between monosulfide solid solution and sulfide melt under controlled oxygen and sulfur fugacities. Geochim Cosmochim Acta 69:4349–4360

Naldrett AJ (1999) World-class Cu-Ni-PGE deposits: key factors in their genesis. Mineral Deposita 34:227–240

Naldrett AJ (2004) Magmatic sulfide deposits: geology, geochemistry and exploration. Springer, Berlin. 728 p

Naldrett AJ (2009) Fundamentals of magmatic sulfide deposits. In: Li C, Ripley E (eds) New developments in magmatic Ni-Cu and PGE deposits. Geological Publishing House, Beijing, pp. 1–26

Ohmoto H, Rye RO (1979) Isotopes of sufur and carbon. In: Barnes HL (ed) Geochemistry of hydrothermal ore deposits, 2nd ed. John Wiley and Sons, London, pp 509–567

Pearce JA (1982) Trace elements characteristics of lavas from destructive plate boundaries. In: Thorpe RS (ed) Andesites: orogenic andesites and related rocks. Wiley, New York, pp. 525–548

Peach CL, Mathez EA, Keays RR (1990) Sulfide melt-silicate melt distribution coefficients for noble metals and other chalcophile elements as deduced from MORB: implications for partial melting. Geochim Cosmochim Acta 54:3379–3389

Peltonen P (1995) Magma-country rock interaction and the genesis of Ni-Cu deposits in the Vammala Nickel Belt, SW Finland. Mineral Petrol 52:1–24

Pirajno F, Mao JW, Zhang ZH, Chai FM (2008) The association of mafic-ultramafic intrusions and A-type magmatism in the Tian Shan and Altay orogens, NW China: implications for geodynamic evolution and potential for the discovery of new ore deposits. J Asian Earth Sci 32:165–183

Qi L, Hu J, Gregoire DC (2000) Determination of trace elements in granites by inductively coupled plasma mass spectrometry. Talanta 51:507–513

Qi L, Zhou MF, Wang CY (2004) Determination of low concentrations of platinum group elements in geological samples by ID-ICP-MS. J Anal At Spectrom 19:1335–1339

Qi L, Zhou MF, Wang CY, Sun M (2007) Evaluation of the determination of Re and PGEs abundances of geological samples by ICP-MS coupled with a modified Carius tube digestion at different temperatures. Geochem J 41:407–414

Qin KZ, Zhang LC, Xiao WJ, Xu XW, Yan Z, Mao JW (2003) Overview of major Au, Cu, Ni and Fe deposits andmetallogenic evolution of the eastern Tianshan Mountains, northwestern China. In: Mao JW, Goldfarb R, Seltmann R, Wang DH, Xiao WJ, Hart C (eds) Tectonic evolution and metallogeny of the Chinese Altay and Tianshan, IAGOD Guidebook Series, London, vol 10, pp. 227–248

Qin KZ, Sun BX, Sakyi PA, Tang DM, Li XH, Sun H, Xiao QH, Liu PP (2011) SIMS zircon U-Pb geochronology and Sr-Nd isotopes of Ni-Cu-bearing mafic-ultrafic intrusions in Eastern Tianshan and Beishan in correlation with flood basalts in Tarim basin (NW China): constraints on a ca. 280 Ma mantle plume. Am J Sci 311: 237–260

Raedeke LD, Mccallum IS (1984) Investigations in the Stillwater Complex: part II. Petrology and petrogenesis of the ultramafic series. J Petrol 25:395–420

Ripley EM (1981) Sulfur isotopic studies of the Dunka Road Cu–Ni deposit, Duluth intrusion, Minnesota. Econ Geol 76:610–620

Ripley EM, Al-Jassar TJ (1987) Sulfur and oxygen isotopic studies of melt-country rock interaction, Babbitt Cu-Ni deposit, Duluth intrusion, Minnesota. Econ Geol 82:87–107

Roeder PL, Emslie RF (1970) Olivine-liquid equilibrium. Contrib Mineral Petrol 29:275–289

San JZ, Qin KZ, Tang DM, Su BX, Sun H, Xiao QH, Liu PP, Cao MJ (2010) Precise zircon U-Pb ages of Tulargen large Cu-Ni-ore bearing mafic-ultramafic complex and their geological implications. Acta Petrol Sin 26:3027–3035 (in Chinese with English abstract)

Sengör AMC, Natal'in BA, Burtman VS (1993) Evolution of the Altaid tectonic collage and Paleozoic crustal growth in Asia. Nature 364: 299–307

Severson MJ, Hauck SA (1990) Geology, geochemistry, and stratigraphy of a portion of the Partridge River intrusion. Technical Report NRRI/GMIN-TR-89-11: 1–152

Song XY, Zhou MF, Cao ZM, Sun M, Wang YL (2003) Ni–Cu–(PGE) magmatic sulfide deposits in the Yangliuping area, Permian Emeishan igneous province, SW China. Mineral Deposita 38:831–843

Song XY, Zhou MF, Tao Y, Xiao JF (2008) Controls on the metal compositions of magmatic sulfide deposits in the Emeishan large igneous province, SW China. Chem Geol 253:38–49

Song XY, Li XR (2009) Geochemistry of the Kalatongke Ni–Cu–(PGE) sulfide deposit, NW China: implications for the formation of magmatic sulfide mineralization in a postcollisional environment. Mineral Deposita 44:303–327

Song XY, Xie W, Deng YF, Crawford AJ, Zheng WQ, Zhou GF, Deng G, Chen SL, Li J (2011) Slab break-off and the formation of Permian mafic-ultramafic intrusions in southern margin of Central Asian Orogenic Belt, Xinjiang, NW China. Lithos 127:128–143

Song XY, Danyushevsky LV, Keays RR, Chen LM, Wang YS, Tian YL, Xiao JF (2012) Structural, lithological, and geochemical constraints on the dynamic magma plumbing system of the Jinchuan Ni–Cu sulfide deposit, NW China. Mineral Deposita 47:277–297

Song XY, Chen LM, Deng YF, Xie W (2013) Syncollisional tholeiitic magmatism induced by asthenosphere upwelling owing to slab detachment at the southern margin of the central Asian Orogenic Belt. J Geol Soc Lond 170:941–950

Su BX, Qin KZ, Sakyi PA, Li XH, Yang YH, Sun H, Tang DM, Liu PP, Xiao QH, Malaviarachchi SP (2011) U-Pb ages and Hf-O isotopes of zircons from Late Paleozoic mafic-ultramafic units in the southern Central Asian Orogenic Belt: tectonic implications and evidence for an Early-Permian mantle plume. Gondwana Res 20:516–531

Su BX, Qin KZ, Su H, Tang DM, Sakyi PA, Chu ZY, Liu PP, Xiao QH (2012) Subduction-induced mantle heterogeneity beneath Eastern Tianshan and Beishan: insights from Nd-Sr-Hf-O isotopic mapping of Late Paleozoic mafic-ultramafic complexes. Lithos 134-135:41–51

Su BX, Qin KZ, Tang DM, Sakyi PA, Liu PP, Su H, Xiao QH (2013) Late Paleozoic mafic-ultramafic intrusions in southern Central Asian Orogenic Belt (NW China): insight into magmatic Ni-Cu sulfide mineralization in orogenic setting. Ore Geol Rev 51:57–73

Sun SS, McDonough W (1989) Chemical and isotopic systematics of oceanic basalts: implications for mantle composition and processes. Geol Soc Lond, Spec Publ 42:313–345

Sun T, Qian ZZ, Deng YF, Li CS, Song XY, Tang QY (2013) PGE and isotope (Hf-Sr-Nd-Pb) constraints on the origin of the Huangshandong magmatic Ni-Cu sulfide deposit in the Central Asian Orogenic Belt, Northwestern China. Econ Geol 108:1849–1864

Tang DM, Qin KZ, Sun H, Su BX, Xiao QH (2012) The role of crustal contamination in the formation of Ni-Cu sulfide deposits in Eastern Tianshan, Xinjiang, Northwest China: evidence from trace element geochemistry, Re-Os, Sr-Nd, zircon Hf-O, and sulfur isotopes. J Asian Earth Sci 49:145–160

Tang DM, Qin KZ, Su BX, Sakyi PA, Liu YS, Mao Q, Santosh M, Ma YG (2013) Magma source and tectonics of the Xiangshanzhong mafic-ultramafic intrusion in the central Asian Orogenic Belt, NW China, traced from geochemical and isotopic signatures. Lithos 170-171:144–163

Thakurta J, Ripley EM, Li CS (2008) Geochemical constraints on the origin of sulfide mineralization in the Duke Island Complex, southeastern Alaska. Geochem Geophys Geosyst 9:Q07003

Theriault RD, Barnes SJ (1998) Compositional variations in Cu-Ni-PGE sulfides of the Dunka Road deposit, Duluth Complex, Minnesota: the importance of combined assimilation and magmatic processes. Can Mineral 36:869–886

Tornos F, Galindo C, Casquet L, Rodríguez PC, Martínez E, Martínez F, Velasco A, Iriondo A (2006) The Aguablanca Ni–(Cu) sulfide deposit, SW Spain: geologic and geochemical controls and the relationship with a midcrustal layered mafic complex. Mineral Deposita 41:737–769

Tyson RM, Chang LLY (1984) The petrology and sulfide mineralization of the Partridge River troctolite, Duluth complex, Minnesota. Can Mineral 22:23–38

Vaillant ML, Saleem A, Barnes SJ, Fiorentini ML, Miller J, Beresford S, Perring C (2016) Hydrothermal remobilization around a deformed and remobilised komatiite-hosted Ni-Cu-(PGE) deposit, Sarah's Find, Agnew Wiluna greenstone belt, Yilgarn Craton, Western Australia. Mineral Deposita 51:369–388

Wang RM, Liu DQ, Ying DT et al (1987) Cu-Ni sulfide deposits in the Tudun-Huangshan region, Hami, Xinjiang: genet controls exploration implications. Miner Rocks 7:1–152 (in Chinese)

Wang YL, Zhang ZW, You MX, Li X, Li K, Wang BL (2015) Chronological and gechemical charcateristics of the Baixintan Ni-Cu deposit in Eastern Tianshan Mountains, Xinjiang, and their implications for Ni-Cu mineralization. Geol China 42:452–467 (in Chinese with English abstract)

Wilson M (1989) Igneous Petrogenesis. Unwin Hyman, London, 466 p

Windley BF, Alexeiev D, Xiao WJ, Kröner A, Badarch G (2007) Tectonic models for accretion of the Central Asian Orogenic Belt. J Geol Soc Lond 164:31–47

Xia MZ, Jiang CY, Li CS, Xia ZD (2013) Characteristics of a newly discovered Ni-Cu sulfide deposit hosted in the Poyi ultramafic intrusion, Tarim Craton, NW China. Econ Geol 108:1865–1878

Xiao WJ, Zhang LC, Qin KZ, Sun S, Li JL (2004) Paleozoic accretionary and collisional tectonics of the Eastern Tianshan (China): implications for the continental growth of central Asia. Am J Sci 304:370–395

Xiao WJ, Han CM, Yuan C, Sun M, Lin SF, Chen HL, Li ZL, Li JL, Sun S (2008) Middle Cambrian to Permian subduction-related accretionary orogenesis of Northern Xinjiang, NW China: implications for the tectonic evolution of central Asia. J Asian Earth Sci 32:102–117

Xiao WJ, Windley BF, Huang BC, Han CM, Yuan C, Chen HL, Sun M, Sun S, Li JL (2009) End-Permian to mid-Triassic termination of the accretionary processes of the southern Altaids: implications for the geodynamic evolution, Phanerozoic continental growth, and metallogeny of Central Asia. Int J Earth Sci 98:1189–1217

Xie W, Song XY, Deng YF, Wang YS, Ba DH, Zheng WQ, Li XB (2012) Geochemistry and petrogenetic implications of a Late Devonian mafic-ultramafic intrusion at the southern margin of the Central Asian Orogenic Belt. Lithos 144-145:209–230

Xie W, Song XY, Chen LM, Deng YF, Zheng WQ, Wang YS, Ba DH, Zhang XQ, Luan Y (2014) Geochemistry insights on the genesis of the subduction-related Heishan magmatic Ni-Cu-(PGE) deposit in Gansu, NW China, at the southern margin of the Central Asian Orogenic Belt. Econ Geol 109:1563–1583

Yang SH, Zhou MF (2009) Geochemistry of the ~430 Ma Jingbulake mafic-ultramafic intrusion in western Xinjiang, NW China: implications for subduction related magmatism in the South Tianshan orogenic belt. Lithos 113:259–273

Yang SH, Zhou MF, Lightfoot PC, Malpas J, Qu WJ, Zhou JB, Kong DY (2012) Selective crustal contamination and decoupling of lithophile and chalcophile element isotopes in sulfide-bearing mafic intrusions: an example from the Jingbulake intrusion, Xinjiang, NW China. Chem Geol 302-303:106–118

Zhang DY, Zhou TF, Yuan F, Fiorentini ML, Said N, Lu YJ, Pirajno F (2013) Geochemical and isotopic constraints on the genesis of the Jueluotage native copper mineralized basalt, Eastern Tianshan, Northwest China. J Asian Earth Sci 73:317–333

Zhang DY, Zhou TF, Yuan F, Fan Y, Deng YF, Xu C, Zhang RF (2014) Genesis of Permian granites along the Kangguer Shear Zone, Jueluotage area, Northwest China: geological and geochemical evidence. Lithos 198-199:141–152

Zhang MJ, Li CS, Fu PE, Hu PQ, Ripley EM (2011) The Permian Huangshanxi Cu-Ni deposit in western China: intrusive-extrusive association, ore genesis, and exploration implications. Mineral Deposita 46:153–170

Zhou MF, Lesher CM, Yang ZX, Li JW, Sun M (2004) Geochemistry and petrogenesis of 270 Ma Ni-Cu-(PGE) sulfide-bearing mafic intrusions in the Huangshan District, eastern Xinjiang, northwest China; implications for the tectonic evolution of the Central Asian orogenic belt. Chem Geol 209:233–257

Zhou TF, Yuan F, Zhang DY, Fan Y, Liu S, Peng MX, Zhang JD (2010) Geochronology, tectonic setting and mineralization of granitoids in Jueluotage area, eastern Tianshan, Xinjiang. Acta Petrol Sin 26:478–502 (in Chinese with English abstract)